

DEPARTAMENT DE QUÍMICA FÍSICA
UNIVERSITAT DE BARCELONA

THEORETICAL STUDY OF THE FLUORINATING POWER
OF SF₆ TO VANADOCENE

Master Thesis of
LUIS MARTÍNEZ SUÁREZ

Màster Oficial en Química Teòrica Computacional

Barcelona, September 2009

The memory entitled “Theoretical study of the fluorinating power of SF₆ to vanadocene” corresponds to the work carried out by Luis Martínez Suárez to obtain the Official Master Title on Computational and Theoretical Chemistry, done in the Departament de Química Física of the Universitat de Barcelona and supervised by Dr. Juan J. Novoa Vide, whom certifies and gives his consent to its presentation.

Dr. Juan J. Novoa Vide

Barcelona, September 2009

INDEX

1. INTRODUCTION	5
2. METHODOLOGY	7
2.1. THE SCHRÖDINGER EQUATION	7
2.2. THE BORN-OPPENHEIMER APPROXIMATION	8
2.3. THE GRADIENT AND THE HESSIAN AS TOOLS FOR THE LOCATION OF MINIMA AND TRANSITION STATES	9
2.4. THE POLYELECTRONIC PROBLEM	11
2.5. THE ANTISYMMETRY PRINCIPLE, THE HARTREE PRODUCT AND THE SLATER DETERMINANT	13
2.6. THE HARTREE-FOCK METHOD	14
2.6.1. THE HARTREE-FOCK LIMIT AND THE CORRELATION ENERGY	16
2.7. THE DENSITY FUNCTIONAL THEORY	17
2.7.1. THE FIRST HOHENBERG-KOHN THEOREM	18
2.7.2. THE SECOND HOHENBERG-KOHN THEOREM	19
2.7.3. THE LEVY'S CONSTRAINED-SEARCH FORMULATION	19
2.7.4. THE KOHN-SHAM METHOD	20
2.7.5. APPROXIMATIONS TO THE EXCHANGE-CORRELATION POTENTIAL	23
2.7.5.1. THE LOCAL DENSITY APPROXIMATION (LDA)	23
2.7.5.2. THE LOCAL SPIN DENSITY APPROXIMATION (LSDA)	24
2.7.5.3. GENERALIZED GRADIENT APPROXIMATIONS (GGA)	24
2.7.5.4. META-GGA FUNCTIONALS	25
2.7.5.5. HYBRID METHODS	25
2.8. ATOMIC BASIS SETS	26
3. REVIEW OF THE LITERATURE: METALLOGENES AND SULFUR	29

HEXAFLUORIDE	
3.1. METALLOCENES: TYPES AND USES	29
3.2. ORBITAL ANALYSIS ON METALLOCENES	31
3.3. STRUCTURAL PARAMETERS OF METALLOCENES	34
3.4. USES AND RISKS OF THE SF ₆	35
3.5. AN ALTERNATING DISSOCIATION ENERGY PATTERN	36
3.6. THE NATURE OF THE S-F BOND ON SF ₆	37
3.7. VANADOCENE FLUORINATION	38
4. PROCEDURE AND RESULTS	40
4.1. GEOMETRY AND ENERGY FOR ISOLATED SPECIES	40
4.2. THE MONO-FLUORINATION REACTION OF THE HIGH SPIN VANADOCENE	45
4.2.1. A THERMODYNAMIC PROFILE	45
4.2.2. A KINETIC PROFILE I. POTENTIAL ENERGY CURVE	49
4.2.3. A KINETIC PROFILE II. POTENTIAL ENERGY SURFACE	51
4.2.3.1. DESIGN OF THE Z-MATRIX	52
4.2.3.2. BUILDING THE POTENTIAL ENERGY SURFACE	53
4.2.3.3. LOCATING THE TRANSITION STATE	56
4.2.4. POTENTIAL ENERGY DIAGRAM FOR THE MONO-FLUORINATION REACTION AT THE 3-21G* LEVEL	57
4.3. A THERMODYNAMIC PROFILE FOR THE BI-FLUORINATION REACTION	58
5. CONCLUSIONS	62
6. BIBLIOGRAPHY	65
7. APPENDICES	71

1. INTRODUCTION

Organometallic halides, and specifically $[\eta^5(\text{C}_5\text{H}_5)_2]\text{M}$ (metallocene) halides, have been found to be of great interest to industry due to their applications in synthesis and in catalysis, and also due to their role as cytostatic and anti-carcinogenic substances. The fluorinated organometallic compounds may present properties of relevant interest in comparison with their chlorinated, brominated and iodinated analogues, in spite of the fact that the last ones have been subject of more attention.

Typically utilized fluorinating agents tend to be hazardous and selective. Finding compounds that can appropriately act as reactants, providing reasonable yields and reaction rates within achievable conditions, as well as minimizing the risks derived from their use, is one of the main interests of chemists. Ernst et. al¹ propose sulfur hexafluoride, SF_6 , as a fluorinating agent from the basis that this compound has been found to react with both early and late low-valent organometallic and inorganic compounds, and experimentally verifies in their work that SF_6 readily acts as a fluorine donor in the reaction with $[\eta^5(\text{C}_5\text{H}_5)_2]\text{V}$, yielding $[\eta^5(\text{C}_5\text{H}_5)_2]\text{VF}$.

In the present work, a theoretical study, performed using Density Functional Theory methods, of the capacity of SF_6 to be a fluorinating agent to vanadocene. Our main aim is, firstly, to determine the thermodynamic and kinetic profile for the forementioned reaction. High spin and low spin states of vanadocene, as well as its high spin and low spin fluorinated derivatives, and the corresponding sulfur fluorides.

The present work is divided in seven chapters, being the first one this introduction. In chapter two, the theoretical background is briefly presented without expanding on the mathematical details underneath it. Chapter three comprises a review of the available references to describe remarkable aspects of the family of molecules that takes part on the studied reactions (i.e. Metallocenes and sulfur fluorides), as well as reported models which, once applied to those compounds, set a basis to understand their properties, structure and reactivity. Chapter four is the main section, explaining the calculations done and their analysis. Chapter five briefly remarks the conclusions that arise from the

discussion in chapter four. Finally, chapter six contains all the external references utilized along the work; and chapter seven, the appendices, includes additional data and information related to the calculations and the discussion that, in spite of not being of a crucial importance to understand this work, contains data that supports the information developed along the discussion. Thus, this work offers an introduction to the fluorination reactions of vanadocene compounds with SF₆, focusing on the mono-fluorination of the high spin vanadocene and obtaining a transition state for this reaction.

2. METHODOLOGY^{2,3}

2.1. THE SCHRÖDINGER EQUATION

According to Quantum Theory, in each instant the state of a system is completely described by a wave function expanded in the Hilbert space, a complex vectorial space which fulfills the properties of the scalar product. Mathematical (and, in most of the cases, Hermitian) operators can be applied over the wave function to obtain properties related to the system. The Hamiltonian operator is of central interest to Quantum Chemistry as it allows to obtain the energy of the system represented by the wave function by means of the time-dependent Schrödinger equation 2.1

$$i\hbar \frac{d|\Psi_t\rangle}{dt} = \hat{H}(t)|\Psi_t\rangle \quad (2.1)$$

However, for Quantum Theory applications involving the study of stationary states, it is possible to consider the time-independent Schrödinger equation 2.2.

$$\hat{H}|\Psi\rangle = E|\Psi\rangle \quad (2.2)$$

Where \hat{H} is the Hamiltonian operator; $|\Psi\rangle$ is a normalized wave-function and E is the energy. Unfortunately, except for the simplest cases, the Schrödinger equation cannot be exactly solved, as will be stated in section 2.3.

The Hamiltonian of a system with nuclei and electrons can be expressed as a sum of different contributions.

$$\hat{H} = \hat{T}_N + \hat{T}_e + V_{NN} + V_{ee} + V_{Ne} \quad (2.3)$$

Where \hat{T}_N is the nuclear kinetic energy operator; \hat{T}_e is the electronic kinetic energy operator, V_{NN} is the internuclear repulsion potential energy, V_{ee} is the interelectronic repulsion potential energy and V_{Ne} is the electron-nucleus attraction potential energy. When replacing each term for the corresponding quantum expression, in atomic units, we obtain expression 2.4

$$\hat{H} = - \sum_{i=1}^n \frac{1}{2} \nabla_i^2 - \sum_{A=1}^M \frac{1}{2M_A} \nabla_A^2 - \sum_{i=1}^n \sum_{A=1}^M \frac{Z_A}{r_{iA}} + \sum_{i=1}^n \sum_{j>i}^n \frac{1}{r_{ij}} + \sum_{A=1}^M \sum_{B>A}^M \frac{Z_A Z_B}{R_{AB}} \quad (2.4)$$

Where i and A are the subscripts for the electrons and the nuclei respectively; M_A and Z_A are respectively the mass and the nuclear charge of the nucleus A ; r_{iA} is the distance from electron i to nucleus A ; and R_{AB} is the distance between nucleus A and nucleus B .

2.2. THE BORN-OPPENHEIMER APPROXIMATION

A central approximation to quantum chemistry is the Born-Oppenheimer approximation, introduced by Max Born and Julius Robert Oppenheimer⁴, based upon the assumption that since nuclei are much heavier than electrons, they move more slowly, and thus the nuclear motion can be separated from the electronic motion, that is, considering the electrons in a molecule to be moving in a field of fixed nuclei. The main point is that the resolution of the system can be done in two different steps that involve the resolution of an electronic problem and a nuclear problem (but, noticeably and against what is used to be stated about the Born-Oppenheimer approximation, those steps are not independent, or the two problems are not *separable*: to solve the nuclear problem, first the electronic problem need to be solved, because the resolution of the electronic problem strongly influences the result obtained from the resolution of the nuclear problem). Equation 2.5 explicitly shows the separation of the total Hamiltonian into a nuclear Hamiltonian and an electronic Hamiltonian.

$$\hat{H} = \hat{H}_{Nuc} + \hat{H}_{el} \quad (2.5)$$

With,

$$\hat{H}_{el} = \hat{T}_e + V_{ee} + V_{Ne} \quad (2.6)$$

$$\hat{H}_{Nuc} = \hat{T}_N + V_{NN} + E_{e,A} \quad (2.7)$$

$E_{e,A}$ is the eigenvalue of the electronic Hamiltonian. The eigenfunction of the electronic Hamiltonian depends explicitly on the electronic coordinates and parametrically on the nuclear coordinates, thus the electronic energy depends on the position of the nuclei,

$$\hat{H}_{el}|\Psi_{el}(\{r_i\};\{R_A\})\rangle = E_{e,A}|\Psi_{el}(\{r_i\};\{R_A\})\rangle \quad (2.8)$$

Where $\Psi_{el}(\{r_i\};\{R_A\})$ is the electronic wave function, which also depends explicitly on r_i and parametrically on R_A , so that can be obtained for fixed values of R_A . The same assumptions can be made to solve the nuclear problem: The eigenfunction of the nuclear Hamiltonian depends explicitly on the nuclear coordinates, as shown in equation 2.9, and for an averaged electron field the motion of the nuclei can be determined.

$$\hat{H}_{Nuc}|\Psi_{Nuc}(\{R_A\})\rangle = E_{tot}|\Psi_{Nuc}(\{R_A\})\rangle \quad (2.9)$$

Thus the Born-Oppenheimer approximation to the total energy includes electronic, vibrational, rotational and translational energy.

The nuclear Hamiltonian can be expressed then, from eq. 2.7, as:

$$\hat{H}_{Nuc} = \hat{T}_N + U(R_A) \quad (2.10)$$

With,

$$U(R_A) = V_{NN} + E_{e,A} \quad (2.11)$$

$U(R_A)$ is a function of the coordinates of the nuclei and is known as the effective potential energy, or potential energy $3N-6$ ($3N-5$ for linear molecules) dimension surface, that determines the motion of the nuclei.

2.3. THE GRADIENT AND THE HESSIAN AS TOOLS FOR THE LOCATION OF MINIMA AND TRANSITION STATES⁵

As was shown in equation 2.10, the energy of a system can be expressed as a function of the nuclear coordinates, giving rise to the concept of potential energy surface. Much of the chemistry involving potential energy surfaces concerns the determination of

minima and first-order saddle points (transition states) through optimization procedures and the evaluation of the gradient and the Hessian. The *gradient* (2.12) is defined as the vector formed by the first derivatives of the potential energy surface with respect to the different nuclear coordinates.

$$\left(\frac{\delta f}{\delta R_1}, \frac{\delta f}{\delta R_2}, \frac{\delta f}{\delta R_3}, \dots, \frac{\delta f}{\delta R_n} \right) \quad (2.12)$$

In a similar way, the *Hessian* (2.13) can be defined as the matrix constructed with the second derivatives of the potential energy surface with respect to all the possible pairs of nuclear coordinates R_i and R_j .

$$\begin{pmatrix} \frac{\delta^2 f}{\delta R_1^2} & \dots & \frac{\delta^2 f}{\delta R_1 \delta R_n} \\ \vdots & \ddots & \vdots \\ \frac{\delta^2 f}{\delta R_n \delta R_1} & \dots & \frac{\delta^2 f}{\delta R_n^2} \end{pmatrix} \quad (2.13)$$

The condition of stationary point is fulfilled when the length of the gradient vector is zero. To evaluate the stationary point, the Hessian matrix must be diagonalized:

- All eigenvalues are positive: Local minimum
- All eigenvalues are negative: Local maximum
- n negative eigenvalues: n th order saddle point. A first order saddle point is a particular case and represents a transition state (a minimum with respect to all the nuclear coordinates except for one of them, along which a maximum is found).

Locating transition states is particularly interesting because of the chemical information about reaction mechanisms they bring and because of the fact that, as unstable species by nature, their experimental determination entails inherent difficulties.

From the mathematical point of view, locating transition states is much more complicated task than finding minima. In order to reach the saddle-point one should start from a sufficiently close geometry. The use of internal coordinates tends to be

helpful because automatically removes the translational and rotational degrees of freedom, and makes also possible to associate the reaction path to one coordinate.

The most commonly employed method is a variation of the Newton-Raphson approach, which, in an iterative procedure, allows to find stationary states of the potential energy surface by solving the system of equations that arises from minimizing the gradient. A starting point with the proper curvature is desirable, and it might be necessary to compute the Hessian at each point during the optimization. Eigenvector following techniques⁶ are less sensitive to the curvature at the starting point, they allow to follow a particular mode associated to the reaction path and can lead to transition states even starting from a wrong geometry.

As it is usually crucial to start from a good initial geometry, there are techniques to obtain reasonable starting approximations to the geometry of the transition state. The Linear Synchronous Transit or LST⁷ is based on the knowledge of the geometries of reactants and products and assumes that the path connecting them is linear as an approximation. The Quadratic Synchronous Transit, in a similar fashion, approximates the reaction path through a parabola.

Different methods employ a LST/QST algorithm to find a starting point, and then the transition state is located by a Newton-Raphson based or an eigenvector method⁸.

2.4. THE POLYELECTRONIC PROBLEM

To evaluate the $U(R_A)$ function for a given set of fixed nuclear coordinates, the electronic problem must be solved by operating the electronic Hamiltonian on its eigenfunctions. For monoelectronic atomic systems, the electronic Hamiltonian is

$$\hat{H}_{el} = \hat{T}_e + V_{Ne} \quad (2.14)$$

And the corresponding eigenfunctions can be exactly determined from equation 2.8. The eigenfunctions obtained from the resolution of a monoelectronic eigenvalues equation corresponding to an atomic system are also called hydrogenoid orbitals, and

can be expressed in a general way as the product of a radial function and a spherical harmonic.

$$\phi(r, \theta, \varphi) = R(r)Y_{l,m}(\theta, \varphi) \quad (2.15)$$

In the case of polyelectronic systems, in addition to the electronic kinetic \hat{T}_e and the electron-nucleus V_{Ne} attraction terms, the interelectronic repulsion V_{ee} term also has to be taken in account. The electronic Hamiltonian \hat{H}_{el} can be then expressed as a sum of a monoelectronic operator which contains the \hat{T}_e and V_{Ne} terms, and a bielectronic operator which accounts for the interelectronic repulsion.

$$\hat{H}_{el} = \hat{T}_e + V_{ee} + V_{Ne} = \sum_{i=1}^n \hat{h}(r_i) + \sum_{i=1}^{n-1} \sum_{j>i}^n \frac{1}{r_{ij}} \quad (2.16)$$

As long as we are concerned with molecular systems, the eigenfunctions of the polyelectronic Hamiltonian will be molecular orbitals. Interelectronic repulsion term in equation 2.16 does not allow the electronic Hamiltonian of a polyelectronic system to be constructed as a finite summatory of monoelectronic terms (that is, only depending on the coordinates of one electron), that is the reason why the exact eigenfunctions cannot be obtained in an easy way from the motioned expression.

Defining a spin orbital $\chi(x)$ as a monoelectronic wave function whose form depends of the position and spin coordinates of an electron (where x stands for both the coordinates of position r and of spin ω), the existence of a complete orthonormal set of an infinite number of spin orbitals can be assumed so that any arbitrary function could be exactly expanded as a linear combination of those spin orbitals, as shown in equation 2.17.

$$f(x) = \sum_{i=1}^{\infty} a_i \chi_i(x) \quad (2.17)$$

Since in practice it is not possible to work with an infinite number of functions, a truncated set of spin orbitals, which would constitute a complete basis set on a determinate subspace, is usually considered as a reasonable approximation to the wave function.

2.5. THE ANTISYMMETRY PRINCIPLE, THE HARTREE PRODUCT AND THE SLATER DETERMINANT

The antisymmetry or Pauli exclusion principle states that *a many-electron wave function must be antisymmetric with respect to the interchange of the coordinate x (both space and spin) of any two electrons*. From the antisymmetry principle is immediately derived the fact that no more than one electron can occupy a spin orbital.

$$\Psi(\mathbf{x}_1, \dots, \mathbf{x}_i, \dots, \mathbf{x}_j, \dots, \mathbf{x}_n) = -\Psi(\mathbf{x}_1, \dots, \mathbf{x}_j, \dots, \mathbf{x}_i, \dots, \mathbf{x}_n) \quad (2.18)$$

Supposing a system in which it is possible to write the exact electronic Hamiltonian in terms of a summatory of one-electron hamiltonians, a possible eigenfunction would be a simple product of spin orbital wave functions describing each electron separately.

$$\Psi^{\text{HP}}(\mathbf{x}_1, \mathbf{x}_2, \dots, \mathbf{x}_n) = \chi_i(\mathbf{x}_1)\chi_j(\mathbf{x}_2) \dots \chi_k(\mathbf{x}_n) \quad (2.19)$$

Such a wave function is called Hartree product, which is an uncorrelated electronic wave function (since the supposed Hamiltonian has no interelectronic repulsion term) and neither takes account of the indistinguishability of electrons nor accomplishes the antisymmetry principle.

To overcome those problems -although not completely- Slater Determinants (normalized and antisymmetrized summatories of Hartree products, all of them composed of the same set of spin orbitals, in which the electron coordinates are permuted in all the possible combinations among the spin orbitals) are extensively used. A short-hand notation for Slater Determinants is shown in expression 2.20.

$$\Psi(\mathbf{x}_1, \mathbf{x}_2, \dots, \mathbf{x}_n) = |\chi_i \chi_j \dots \chi_k\rangle \quad (2.20)$$

A Slater Determinant incorporates *exchange correlation*, which means that the motion of two electrons with parallel spin is correlated. However, the motion of electrons of opposite spin remains uncorrelated, so that there is a finite possibility of finding two electrons with opposite spins at the same point of space simultaneously.

Physically, a Slater Determinant represents a specific electronic state in an electronic system, and a linear combination of different Slater Determinants could be able to

represent a system in which different electronic states are considered, although an exact solution for those polyelectronic systems would nevertheless involve an infinite number of spin orbitals, as long as an infinite number of Slater Determinants (eq. 2.21 –see also Figure 2.1-).

$$\Phi(x_1, x_2, \dots, x_n) = \sum_{i=1}^{\infty} \sum_{j>i}^{\infty} \dots \sum_{k>\dots>j>i}^{\infty} c_{ij\dots k} |\chi_i \chi_j \dots \chi_k\rangle \quad (2.21)$$

2.6. THE HARTREE-FOCK METHOD

The Hartree-Fock method is a single-referent method that uses a wave function composed of only one Slater Determinant to solve the eigenvalues problem for an exact polyelectronic Hamiltonian. Since for polyelectronic systems the exact wave function is not known, also makes use of a truncated set of spin orbitals. The variational principle states that the n th eigenvalue of an operator applied on a truncated (incomplete) basis set of functions is always larger in value than the n th eigenvalue of the same operator applied on the exact function (or a complete set of functions), thus the wave function that can represent an electronic system in a better way will be the one that gives a set of eigenvalues as low as possible, minimizing equation 2.22.

$$E_0 = \langle \Psi_0 | \hat{H} | \Psi_0 \rangle \quad (2.22)$$

The intermediate steps to obtain the result will not be detailed here, as they are extensively explained in other sources^{2,3,9}, but the spin orbitals obtained from minimizing the value of E_0 are the eigenfunctions of a mono-electronic operator known as the Fock operator $\hat{f}(\mathbf{x})$.

$$\hat{f}(\mathbf{x}) \equiv \hat{h}(\mathbf{x}) + \hat{v}_e(\mathbf{x}) \quad (2.23)$$

$\hat{h}(\mathbf{x})$ is a mono-electronic operator already defined in 2.16, and $\hat{v}_e(\mathbf{x})$ is an effective interelectronic repulsion mono-electronic operator.

$$\hat{v}_e(\mathbf{x}) = \sum_{i=1}^n \hat{j}_i(\mathbf{x}) - \hat{k}_i(\mathbf{x}) \quad (2.24)$$

\hat{j} and \hat{k} are the coulomb and exchange operators respectively, and through they are formally mono-electronic operators, their expected values are the bi-electronic integrals shown in equations 2.25 and 2.26 (they are also shown in Dirac's notation).

$$\langle \chi_j(\mathbf{x}_1) | \hat{j}_i(\mathbf{x}_1) \chi_j(\mathbf{x}_1) \rangle = \int \chi_i^*(\mathbf{x}_1) \chi_j^*(\mathbf{x}_2) r_{12}^{-1} \chi_i(\mathbf{x}_1) \chi_j(\mathbf{x}_2) d\mathbf{r}_1 d\mathbf{r}_2 = \langle ij || ij \rangle = J_{ij} \quad (2.25)$$

$$\langle \chi_j(\mathbf{x}_1) | \hat{k}_i(\mathbf{x}_1) \chi_j(\mathbf{x}_1) \rangle = \int \chi_i^*(\mathbf{x}_1) \chi_j^*(\mathbf{x}_2) r_{12}^{-1} \chi_j(\mathbf{x}_1) \chi_i(\mathbf{x}_2) d\mathbf{r}_1 d\mathbf{r}_2 = \langle ij || ji \rangle = K_{ij} \quad (2.26)$$

The coulomb integral 2.25 represents classical coulombic repulsion between electrons described by spin orbitals i and j , the exchange integral 2.26 arises from the antisymmetrized nature of the Slater determinant and does not have a simple classical interpretation.

Obtaining the eigenvalues of the Fock operator $\hat{f}(\mathbf{x})$ is an iterative process since the $\hat{v}_e(\mathbf{x})$ operator depends on the eigenfunctions. That iterative procedure is called the self-consistent-field (SCF) method. The Hartree-Fock equation 2.27

$$\hat{f}(\mathbf{x}_i) \chi(\mathbf{x}_i) = \epsilon \chi(\mathbf{x}_i) \quad (2.27)$$

must be solved by introducing an initial guess to the eigenfunctions of $\hat{f}(\mathbf{x}_i)$, that can be the eigenfunctions of the $\hat{h}(\mathbf{x}_i)$ operator, from which a first guess of $\hat{v}_e(\mathbf{x}_i)$ can be calculated, and then use it to calculate a new set of eigenfunctions of $\hat{f}(\mathbf{x}_i)$. When the difference obtained (for example of the E_0 or the ϵ values) between two consecutive cycles is smaller than a previously defined cut-off for the error, the best guess for the eigenvalues of the Fock operator is obtained.

2.6.1. THE HARTREE-FOCK LIMIT AND THE CORRELATION ENERGY

Larger basis sets will give lower energy values until the so known as Hartree-Fock limit is reached (with an infinite basis set). That energy is the best approach to the exact energy that can be obtained from the Hartree-Fock method. The difference between the Hartree-Fock limit and the exact energy is the correlation energy, which has a negative value since the exact energy is always smaller (larger in absolute value) than the Hartree-Fock energy.

$$E^{\text{corr}} = E^{\text{exact}} - E^{\text{HF}} < 0 \quad (2.28)$$

This correlation energy arises directly from the fact that the Hartree-Fock method, although including correlation between electrons of the same spin coordinate (which is known as Fermi hole), does not include correlation between electrons of different spins (which is known as Coulomb hole). The total energy obtained for a polyelectronic system can still be improved through wave function based methods by multi-configurational procedures that introduce the wave function as the expansion of more than one Slater Determinant (eq. 2.21 shows an expression for a Full-CI expansion, which contains an infinite number of determinants), and are called *Post Hartree-Fock* methods (Configuration Interaction, Coupled Cluster, Perturbation Theory and Møller-Plesset partition) if they include the correlation energy *after* a set of spin orbitals has been optimized, and the *Multi-Configurational* methods (MCSCF, CASSCF, MRCI, CASPT2...) which allow to optimize variationally at the same time the set of spin orbitals and the set of electronic configurations. However, those methods will not be introduced in this work. For further references to Post Hartree-Fock and Multi-Configurational methods see the literature^{5,10,11,12}.

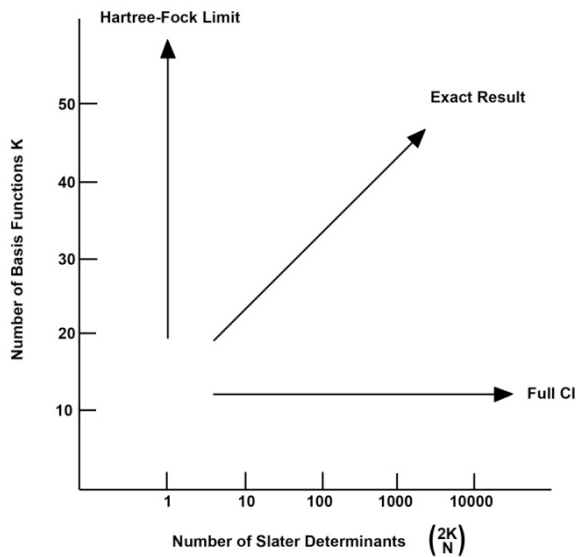


Figure 2.1 Dependence of calculations on size of one-electron and N-electron basis sets.

2.7. THE DENSITY FUNCTIONAL THEORY^{5,9}

While the Hartree-Fock method is a wave function-based method, we will introduce now the Density Functional Theory, an electronic density-based method generally more computationally efficient than wave function-based methods. Although its predecessor can be found in the Thomas-Fermi model^{13,14}, DFT formalism arose from the Hohenberg-Kohn theorems¹⁵ and was explicitly developed by Walter Kohn and Lu Jeu Sham with the Kohn-Sham method¹⁶.

The electron density $\rho(\mathbf{r}_1)$ is defined as the number of electrons within the volume defined by \mathbf{r}_1 and $\mathbf{r}_1 + d\mathbf{r}_1$ in a given state. It can be calculated from the wave function of the system with equation 2.27.

$$\rho(\mathbf{r}_1) = N \int \dots \int |\Psi(\mathbf{x}_1, \mathbf{x}_2, \dots, \mathbf{x}_N)|^2 d\mathbf{s}_1 d\mathbf{x}_2 \dots d\mathbf{x}_N \quad (2.29)$$

And it integrates over all the space to give the total number of electrons N.

$$\int \rho(\mathbf{r}) d\mathbf{r} = N \quad (2.30)$$

2.7.1. THE FIRST HOHENBERG-KOHN THEOREM

The first Hohenberg-Kohn Theorem legitimizes the use of the electron density $\rho(\mathbf{r})$ as a basic variable instead of the wave function to determine a polyelectronic system. It states: *The external potential $v(\mathbf{r})$ is determined, within a trivial additive constant, by the electron density $\rho(\mathbf{r})$.* It can be seen from the general expression of the Hamiltonian of a polyelectronic system (2.16) that the external potential $v(\mathbf{r})$ completely determines its form. $\rho(\mathbf{r})$ also determines the number of electrons, so the system in its ground state is completely determined by $\rho(\mathbf{r})$. Another way to state the first Hohenberg-Kohn Theorem is: *Any observable of a stationary non-degenerate ground state can be calculated, exactly in theory, from the electron density of the ground state. In other words, any observable can be written as a functional of the electron density of the ground state.* Thus the energy can be expressed as a functional of the density:

$$E[\rho] = T[\rho] + V_{Ne}[\rho] + V_{ee}[\rho] (+V_{NN}) \quad (2.31)$$

Where $T[\rho]$ and $V_{ee}[\rho]$ are universal functionals, the kinetic energy density functional and the interelectronic repulsion density functional respectively, usually encompassed within the Hohenberg-Kohn functional $F_{HK}[\rho]$. Within this consideration the eq. 2.31 can be rewritten as:

$$E_v[\rho] = \int \rho(\mathbf{r})v(\mathbf{r})d\mathbf{r} + F_{HK}[\rho] \quad (2.32)$$

There is a direct relation between the density and the wave function through the external potential:

$$\rho(\mathbf{r}) \rightarrow v(\mathbf{r}) \rightarrow \hat{H} \rightarrow \Psi \quad (2.33)$$

That implies that $\rho(\mathbf{r})$ must be N-representable (i.e. must be a positive function defined in the entire space and its integral must be equal to the total number of electrons) and v-representable (i.e. there is an external potential from which $\rho(\mathbf{r})$ can be derived).

2.7.2. THE SECOND HOHENBERG-KOHN THEOREM

The second theorem of Hohenberg-Khon provides de energy variational principle and states that: *The electron density of a non-degenerate ground state can be calculated, exactly in theory, determining the density that minimizes the energy of the ground state* (eq. 2.34). This principle assures that any trial density ρ results in an energy greater or equal to the exact energy of the ground state.

$$\left[\frac{\delta E_v[\rho]}{\delta \rho} \right] = 0 \quad (2.34)$$

2.7.3. THE LEVY'S CONSTRAINED-SEARCH FORMULATION

In the Hohenberg-Khon formulation, the one-to-one map cannot be directly established between ρ and Ψ , given that when passing through an identical potential (e.g. in a degenerate ground state), the connection is lost. Levy's constrained-search formulation¹⁷ allows a one-to-one map between ρ and Ψ without passing through $v(\mathbf{r})$ (i.e. $p(\mathbf{r})$ is not required to be v -representable), and the formulation can also be applied to degenerate ground states since they are described by different wave functions. Given a set of functions $\{\Psi_{\rho_0}\}$ that integrate to ρ_0 , the exact density for a given ground state, it is demonstrated by the variational principle that,

$$F_{\text{HK}}[\rho] = \min_{\Psi \rightarrow \Psi_{\rho_0}} \langle \Psi | \hat{T} + \hat{V}_{ee} | \Psi \rangle \quad (2.35)$$

The Ψ_0 is the one that minimizes the expected value of $\hat{T} + \hat{V}_{ee}$.

In principle, excited states of a given symmetry and/or spin can be studied restricting the set of functions used in the variational procedure to suitable symmetry and spin multiplicity functions, using the same arguments as in the Levy's constrained-search formulation, however it is demonstrated¹⁸ that for a given excited state there might exist more than one external potential which yields the electron density of that state, and consequently the energy of the excited state would not be a functional of the density.

To assure the N-representability while applying the variational procedure to a problem, a restriction is introduced via undetermined Lagrange multipliers,

$$\delta \left[E_v[\rho] - \mu \left(\int \rho(r) dr - N \right) \right] = 0 \quad (2.36)$$

The Lagrange multiplier μ has the meaning of a chemical potential. From equation 2.36, equation 2.37 can be obtained and is known as the *fundamental equation of density functional theory*.

$$\mu = \frac{\delta E_v[\rho]}{\delta \rho(r)} = v(r) + \frac{\delta F_{\text{HK}}[\rho]}{\delta \rho(r)} \quad (2.37)$$

Equation 2.37 is easily obtained from combining equations 2.32 and 2.36.

2.7.4. THE KOHN-SHAM METHOD

The main problem in solving equation 2.37 is that the exact expression relating F_{HK} with the density is unknown. The Kohn-Sham method¹⁹ proposes a way to overcome this problem using a *reference system* of non-interacting N electrons that move under the same external potential $v(r)$ as the real system, as an initial guess (in a similar way to the Hartree-Fock method). The Hamiltonian of such a system only contains single-electron terms:

$$\tilde{H}_s = \sum_{i=1}^n \hat{h}(i) = \sum_{i=1}^n -\frac{1}{2} \nabla^2(i) + \sum_{i=1}^n \hat{v}_s(i) \quad (2.38)$$

For Hamiltonian in 2.38 the exact wave function can be calculated, and subsequently the exact density and kinetic energy can also be exactly calculated through 2.39 and 2.40 respectively.

$$\rho(r) = \sum_{i=1}^{n_{occ}} |\chi_i(r)|^2 \quad (2.39)$$

$$T_s[\rho] = \sum_{i=1}^{n_{occ}} \left\langle \chi_i \left| -\frac{1}{2} \nabla^2 \right| \chi_i \right\rangle \quad (2.40)$$

For the *reference system*, the energy can thus be expressed starting from equation 2.31 and obtaining a similar expression than that of equation 2.32:

$$E_v[\rho] = \sum_{i=1}^{n_{occ}} \varepsilon_i = T_s[\rho] + \int \rho(r) v_s(r) dr \quad (2.41)$$

The subscript *s* indicates that we are considering the *reference system*. In the real system, in which the *N* electrons interact, the energy can be expressed as:

$$E_v[\rho] = T[\rho] + \int \rho(r) v(r) dr + V_{ee}[\rho] \quad (2.42)$$

If a partition is done in the expression of the energy between the *reference system* terms and the real system terms, the energy of the real system can be expressed:

$$E_v[\rho] = T_s[\rho] + \int \rho(r) v(r) dr + J[\rho] + (T[\rho] - T_s[\rho]) + (V_{ee}[\rho] - J[\rho]) \quad (2.43)$$

$J[\rho]$ is the Coulomb repulsion energy, the term $T[\rho] - T_s[\rho] = T_c[\rho]$ is known as the correlation kinetic energy, and the term $V_{ee}[\rho] - J[\rho] = W_{xc}[\rho]$ is the exchange-correlation energy of the electronic part. These two contributions are usually grouped in

one single term, $E_{xc}[\rho]$, called total exchange-correlation energy, which contains all the contributions to the energy for which we do not have a simple expression as a function of the electron density. The resulting energy equation is:

$$E_v[\rho] = T_s[\rho] + \int \rho(r)v(r)dr + \frac{1}{2} \iint \frac{\rho(r_1)\rho(r_2)}{|r_1 - r_2|} dr_1 dr_2 + E_{xc}[\rho] \quad (2.44)$$

Applying 2.44 to 2.37, and in an iterative process (resembling that of the SCF), from the initial guess of spin orbitals obtained from the resolution of the eigenvalues equation of the Hamiltonian of the *reference system* (see eq. 2.38) an initial guess for the electron density can be obtained directly from equation 2.35; and from electron density the $v_{eff}(r)$ can be obtained from equation 2.45, which arises from derivating with respect to $\rho(r_1)$ all the contributions to the potential energy present in eq. 2.44 (that is, all the terms except the un-correlated kinetic energy functional $T_s[\rho]$).

$$v_{eff}(r) = v(r) + \int \frac{\rho(r_2)}{|r_1 - r_2|} dr_2 + \frac{\delta E_{xc}[\rho]}{\delta \rho(r)} \quad (2.45)$$

Making use of equation 2.45, the Kohn-Sham monoelectronic Hamiltonian can be written for the real system:

$$\hat{h}_{KS} = -\frac{1}{2}\nabla^2 + v_{eff}(r) \quad (2.46)$$

And from the corresponding eigenvalues equation (2.47) the Kohn-Sham orbitals can be obtained.

$$\hat{h}_{KS}\chi_i = \varepsilon_i\chi_i \quad (2.47)$$

The orbitals that appear in equation 2.47 are the Kohn-Sham orbitals and, though they do not have strict physical meaning, they can be used for reactivity studies, given that their shape, symmetry and energetic order has been proved to coincide with those of the Hartree-Fock calculations¹⁶.

2.7.5. APPROXIMATIONS TO THE EXCHANGE-CORRELATION POTENTIAL

Since an exact expression to $E_{xc}[\rho]$ in eq. 2.44 is not known, good approximations are needed to put DFT into practice. Different ways of doing that are described hereafter, from simplest LDA to the more complex hybrid functionals.

2.7.5.1. THE LOCAL DENSITY APPROXIMATION (LDA)

The Local Density Approximation, or LDA, supposes that exchange and correlation energy depend only on the local density (i.e. the density in an infinitesimal volume). The function $\varepsilon_{xc}[\rho]$ is introduced as the exchange and correlation energy per particle, which depends exclusively on a constant density ρ ; while $E_{xc}^{LDA}[\rho]$ can be expressed as:

$$E_{xc}[\rho] = \int \rho(r) \varepsilon_{xc}[\rho] dr \quad (2.48)$$

$\varepsilon_{xc}[\rho]$ can be separated into exchange and correlation contributions:

$$\varepsilon_{xc}^{LDA}[\rho] = \varepsilon_x^{LDA}[\rho] + \varepsilon_c^{LDA}[\rho] \quad (2.49)$$

The exchange part can be expressed²⁰ as

$$\varepsilon_x^{LDA}[\rho] = -\frac{9}{4}\alpha \left(\frac{3}{8\pi}\right)^{\frac{1}{3}} \rho^{\frac{1}{3}} \quad (2.50)$$

where α is an adjustable parameter²¹.

For the correlation energy different approaches exist^{22,23,24} but it is difficult to obtain separately from the exchange energy. This is normally achieved by using a suitable interpolation formula, starting from a set of values calculated for a number of different densities in an homogeneous electron gas²⁵.

2.7.5.2. THE LOCAL SPIN DENSITY APPROXIMATION (LSDA)

In open-shell systems, since the densities of α and β electrons are different, they must be treated separately. In the same way as in LDA, exchange correlation energy can be separated into two contributions:

$$E_{XC}^{LSDA}[\rho^\alpha] = E_X^{LSDA}[\rho^\alpha] + E_C^{LSDA}[\rho^\alpha, \rho^\beta] \quad (2.51)$$

Exchange only depends on ρ^α density because there is not exchange contribution between electrons of different spin coordinate. Both contributions can be treated in a similar way as are in LDA.

LDA functionals yield good geometries, good vibrational frequencies and reasonable charge densities, except in the regions close to the nuclei; but have a general tendency to exaggerate the strength of the bonds and are not suitable for systems with weak bonds.

2.7.5.3. GENERALIZED GRADIENT APPROXIMATIONS (GGA)

GGA introduces density gradients into the description of exchange and correlation effects, taking into account not only the value of the density in each point but also its variation $\nabla\rho$.

$$E_{XC}^{GGA}[\rho] = \int f(\rho, \nabla\rho) dr \quad (2.52)$$

Becke's non-local correction to the exchange²⁶ adds a non-local term to the LDA expression:

$$E_X^{GGA}[\rho] = E_X^{LDA}[\rho] + E_X^{NLDA}[\rho] \quad (2.53)$$

With,

$$E_X^{NLDA}[\rho] = \int \rho^{\frac{4}{3}}(r) f^{NLDA}(x) dr \quad (2.54)$$

Where $f^{NLDA}(\mathbf{x})$ is a parametrized function of the density and its gradient which gives a correct asymptotic behaviour of the exchange energy per particle. Many other non-local corrections are used, but the most often used are perhaps the Becke's²⁶ correction to the exchange and those of Perdrew²⁷ and Lee, Yang and Parr²⁸ to the correlation. Those functionals still fail to describe van der Waals complexes.

2.7.5.4. META-GGA FUNCTIONALS

In meta-GGA functionals, the exchange and correlation energy functional contains not only the density and its gradient, but also the kinetic energy density $\tau(\mathbf{r})$, which depends on the occupied kohn-sham orbitals, and/or the Laplacian of the density $\nabla^2\rho$ ²⁹.

$$E_{XC}^{meta-GGA}[\rho] = \int f(\rho, \nabla\rho, \tau, \nabla^2\rho) dr \quad (2.55)$$

The presence of second derivatives requires a larger computational effort. Examples of meta-GGA functionals include B95³⁰, KCIS³¹, TPSS³² and VSXC³³.

2.7.5.5. HYBRID METHODS

Hybrid density functional (H-GGA) methods combine the exchange-correlation of a conventional GGA method with a percentage of Hartree-Fock (or exact) exchange.

$$E_{XC}[\rho] = \int_0^1 W_{XC}^\lambda[\rho] d\lambda \quad (2.56)$$

Expression 2.56 makes up the so-called adiabatic connection, in which a value $\lambda = 0$ represents Hartree-Fock exchange, and for $\lambda = 1$ the exchange energy is approximated by a LSDA or GGA functional.

The exact amount of Hartree-Fock exchange cannot be assigned from first-principles and therefore is fitted semi-empirically. Hybrid functionals allow a significant improvement over GGAs for many molecular properties and they have become widely used²⁵ (although in solid-state physics this type of functional is much less successful due to difficulties on computing the exact-exchange part within a plane-wave basis set). Examples of hybrid functionals include B3LYP^{26,28,30}, B3P86^{26,27,30}, B3PW91^{26,30,34}, etc. The B3LYP functional, whose expression is shown in equation 2.57,

$$E_{XC} = E_X^{LSDA} + a_0(E_X^{exact} - E_X^{LSDA}) + a_x \Delta E_X^{B88} + E_C^{VWN} + a_c(\Delta E_C^{LYP} - E_C^{VWN}) \quad (2.57)$$

shows a local LSDA correction to exchange (E_X^{LSDA}), a parametrized amount of exact exchange [$a_0(E_X^{exact} - E_X^{LSDA})$], a B88 non-local correction to exchange ($a_x \Delta E_X^{B88}$), a local VWN correction to correlation (E_C^{VWN}) and a non-local LYP correction to correlation [$a_c(\Delta E_C^{LYP} - E_C^{VWN})$]. This functional is one of the most widely used in DFT calculations, with an estimated use of about the 80% over all the other functionals²⁵.

The hybrid meta-GGA functionals combine meta-GGA functionals with Hartree-Fock exchange, and represent a new class of density functionals nowadays under active development.

2.8. ATOMIC BASIS SETS⁵

Within LCAO formulation, to describe mathematically spin orbitals, the definition of a set of functions to expand their spatial part is required, according to eq. 2.58.

$$\varphi_i = \sum_{\mu} c_{\mu i} \phi_{\mu} \quad (2.58)$$

φ_i is the spatial part of the i th spin orbital, $c_{\mu i}$ are the coefficients of the lineal expansion and ϕ_{μ} are a set of atomic basis functions, or *atomic basis set*. Slater-type orbitals (STO) (2.59) are simpler than hydrogen-like orbitals, but describe well the zone of the nucleus. However, the calculation of tri- and tetracentric integrals is not analytical.

$$\phi_{\zeta,n,l,m}(r, \theta, \varphi) = Nr^{n-1}e^{-\zeta r}Y_{l,m}(\theta, \varphi) \quad (2.59)$$

An alternative to STO are Gaussian-type orbitals (GTO), which can be expressed as in eq. 2.60. All the integrals arising from those orbitals can be calculated analytically, in spite that GTO do not behave as well as STO near the nucleus.

$$\phi_{\zeta,n,l,m}(r, \theta, \varphi) = Nx^l x^l y^l z^l e^{-\zeta r^2} \quad (2.60)$$

Pople and co-workers developed STO-NG basis sets to combine the advantages of the two types of functions. STO-NG are Slater-type orbitals constructed as a least squares fitting of an expansion of N Gaussian functions (eq. 2.61). The most widely used of such expansions is STO-3G. These types of expansions are usually called *contracted Gaussian functions*, and the Gaussian functions used on the contraction are called *primitive Gaussian functions*.

$$\phi_{STO-NG} = \sum_i^N a_i g_i \quad (2.61)$$

The minimal basis set, namely the one that contains only the basis functions necessary to describe the occupied orbitals of a system on its ground state, is for most of the cases not flexible enough. Some ways of increasing the flexibility of the basis set are doubling the number of orbitals, which leads to the *Double Z* basis sets; or the more economical *split-valence* basis sets, which split only the valence orbitals and were proposed also by Pople and co-workers. An example of a split-valence basis set is 3-21G, where each inner electron is described by one STO built from three primitive Gaussian functions, and each valence electron is described by two STO, one of which is built from two primitive Gaussian functions and the other one is built from only one primitive Gaussian function.

To include polarization effects on electrons, *polarization functions* are added to the basis set. These functions have a higher angular momentum than the occupied valence orbitals of the atom. Polarization functions would be of *p* type for a hydrogen atom, but of *d* type for an element of the second row, with *p* functions in its valence shell. The inclusion of polarization functions is represented with a * sign or alternatively with a (d).

To describe electrons located far from the nucleus, for example valence electrons of anions, *diffuse functions* are added to the basis set. Those functions have very small

exponents, allowing the probability of finding electrons far from the nucleus increase just by increasing the contribution of the diffuse functions.

3. REVIEW OF THE LITERATURE ON METALLOCENES AND SULFUR HEXAFLUORIDE

The chemical reaction of vanadocene [bis(cyclopentadienyl)vanadium, $V(C_5H_5)_2$] with the SF_6 gas has been proven experimentally by Ernst et al¹ to yield its mono-fluorinated derivative, the previously unreported paramagnetic 16-electron (fluoro)bis(cyclopentadienyl) vanadium, $V(C_5H_5)_2F$. They obtained $V(C_5H_5)_2F$ dissolving sublimed $V(C_5H_5)_2$ in toluene, and then bubbling SF_6 through the solution at ambient temperature. The solution gradually lightened its color to a pale purple. When filtered, concentrated and recrystallized, blue plates were obtained with a yield of the 58%.

This section will introduce the molecules intervening on the reaction of study, namely the vanadocene complexes and the sulfur fluorides. Vanadocenes can be understood in the more general frame of the metallocene complexes. A brief glimpse to the many uses of those compounds will be presented, as well as an explanation of some of their properties through the molecular orbital theory. An analogous introduction to sulfur hexafluoride and its derivatives will follow.

3.1. METALLOCENES: TYPES AND USES

The metallocene chemistry raised as an active field of chemistry after the discovery of ferrocene in 1951, whose structural and bond properties³⁵ earned a Nobel prize to Fischer and Wilkinson and established the study of metal-carbon bonds as an independent discipline known today as organometallic chemistry. Subsequently to that discovery followed the development of a metallocene chemistry for most of the d-elements. Strictly speaking, metallocenes are “sandwich” compounds involving two cyclopentadienyl (Cp) rings and a metallic center, and are expressed by the formula $[M(\eta^5C_5H_5)_2]$. The name of metallocene is nowadays also applied to other related compounds (Fig. 3.1). Examples include bent metallocenes, which contain further ligands attached to the metallic center; ansa-metallocenes, with a bridge between the two Cp rings; metallocenes in which one or more hydrogens of the Cp rings have been

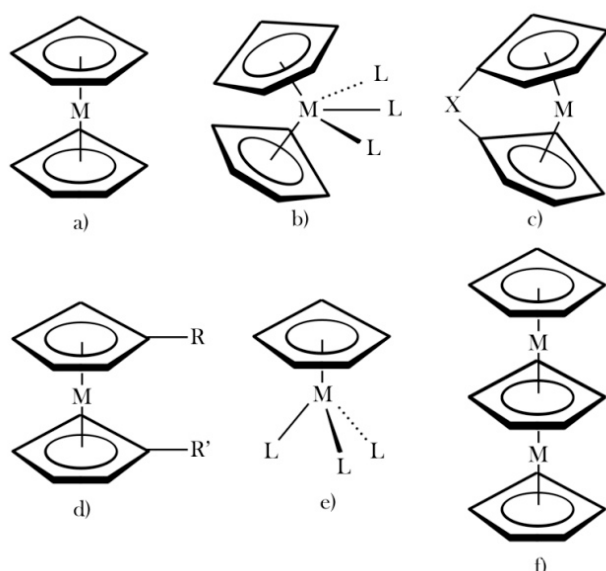


Fig. 3.1 Some general structures for metallocenes. a) metallocene with parallel Cp rings, b) bent metallocene with ligands, c) ansa-metallocene, d) Cp substituted metallocene, e) half-sandwich and f) multidecker sandwich.

substituted by other species; “half sandwich” metallocenes, or cyclopentadienyl complexes, with one of the Cp rings substituted by a different ligand; “multidecker sandwiches”, or multicyclopentadienyl complexes; and several more possible structures involving metallic complexes with one or more Cp rings as ligands, such as ions or polymers.

Metallocene compounds have a wide and important applicability in industry as catalysts. Bis(cyclopentadienyl)group IV metal complexes, mainly zirconocene complexes, have been found to act as catalysts on Ziegler-Natta homogeneous polymerization of alkenes³⁶ to synthesize polymers which cannot be produced by conventional Ziegler-Natta catalysts. Ansa-metallocenes have found extensive use as catalysts that effect enantioselective bond-forming processes³⁷, due to their geometrically constrained structure³⁸. In antisymmetric homogeneous catalysis, ferrocenyl ligands (ferrocene complexes with one or more substituents in the Cp rings) represent an important class of auxiliaries that find application in processes such as Rh-catalyzed hydrogenation in the synthesis of biotin³⁹ or Ir-catalyzed ketimine hydrogenation to generate the herbicide (S)-metolachlor⁴⁰.

Metallocenes have been of proved interest in other fields also. Bent metallocene complexes with two halides containing Ti, V, Nb or Mo as central atoms have been reported to have strong antitumor properties⁴¹, particularly cytostatic activity of titanocene complexes is known since 1979⁴². Vanadocene(IV) complexes of general formula Cp_2VX_2 (X=halide, pseudohalide) have also been found to have spermicidal properties⁴³. $TCNE^-$ and $TCNQ^- VCp_2$ complexes have been studied by Choukroun et al.⁴⁴ among others due to its potential use as molecular magnet building blocks. Metallocene-based polymers, known shortly after the discovery of ferrocene⁴⁵, such as organic polymers with metallocene side groups, poly(metallocenes) or even dendritic

poly(metallocenes) are also being studied, as well as the synthetic ways that lead to their obtention.

In addition to these uses, many other applications for metallocenes and metallocene derivatives are known, and represent actual subjects of research⁴⁶⁻⁵¹.

3.2. ORBITAL ANALYSIS ON METALLOCENES

The structure and chemistry of the first transition metal series varies widely and is dominated by the number of valence electrons each compound possesses⁴⁵. Ferrocene has a stable 18-electron configuration, but the reactivity of the metallic center increases when the number of valence electrons changes. E.g. Vanadocene is a 15 electron structure with three unpaired electrons, very air sensitive in solution and in solid state, highly reactive and acting like a carbene in some respects. Chromocene is unstable and air sensitive. Manganocene has significant ionic character and is quite reactive to atmospheric oxygen, yielding ferrocene when it reacts with FeCl_2 in THF. Cobaltocene is a powerful reducing agent that undergoes electrophilic substitution reactions to form cobaltocenium salts or substituted cyclopentadiene complexes. Nickelocene is also easily oxidized and its reactivity reflects the tendency to achieve 18-electron configuration. From experimental facts and theoretical studies it seems clear that reactivity for ferrocene is the lower one and it increases changing the coordination metal atom.

A proper way to understand the structures and reactivities of the $[\text{M}(\eta^5\text{C}_5\text{H}_5)_2]$ metallocenes (shortened to MCp_2 from now on) is by analyzing the energy and symmetry of their molecular orbitals and their electronic structure. From a molecular orbital analysis comes out that MCp_2 complexes are better understood as an octahedron rather than a two coordinate or ten coordinate complex, because Cp^- ligands have six π -electrons and utilize three coordination sites⁵⁴. In Fig. 3.2 it can be seen that the frontier molecular orbitals correspond to an almost triply degenerate set of a_{1g} and e_{2g} symmetry, mainly formed by the xy , x^2-y^2 , and z^2 d orbitals of the metal. Above them two degenerate e^*_{1g} orbitals arising from the anti-bonding overlap of the xz and yz d orbitals of the metal and the Cp rings molecular orbitals of the same symmetry are

located. A very similar splitting can be observed in a typical octahedral complex, with a degenerate set of three non-bonding metal d-orbitals with t_{2g} symmetry and two anti-bonding $2e_g$ orbitals.

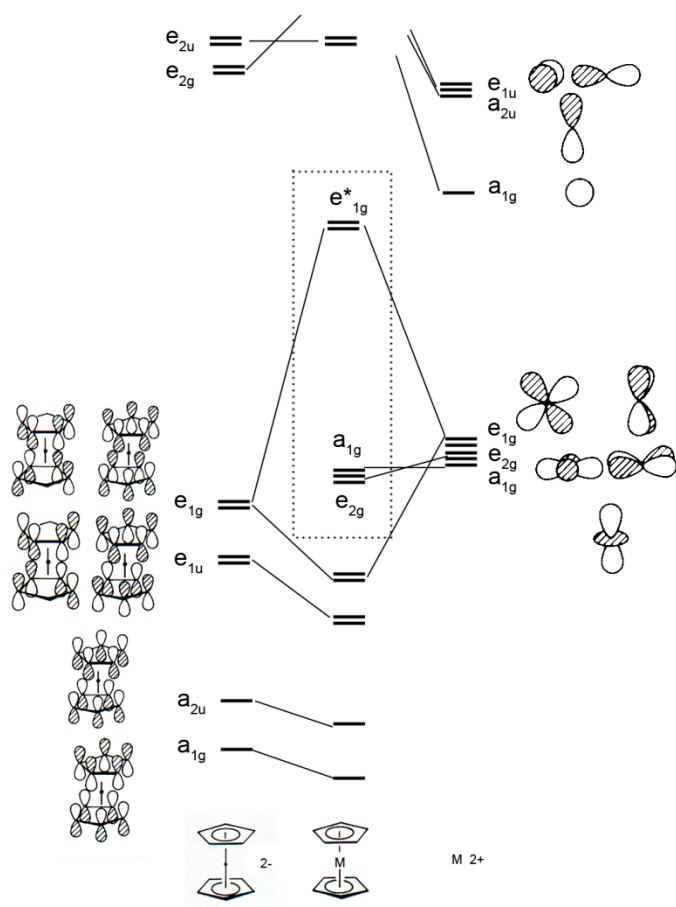


Fig. 3.2 Molecular orbital diagram for metallocene as a combination of two parallel cyclopentadienyl rings and a transition metal. The molecular orbitals inside the dotted box indicate the frontier orbitals (those occupied by the d electrons of the metal)⁵⁴.

In the case of ferrocene, the three frontier orbitals are doubly occupied, while in the case of vanadocene, there would be three available electrons to fill the a_{1g} and the two e_{2g} frontier orbitals, giving rise to different possible multiplicities (a quartet and a doublet). In general, in the MCp_2 metallocenes in which two states with different multiplicities are possible, the lower energy state is that of maximum multiplicity. This trend is expected to be greater for the first transition metals than for the second transition metals, because of their stronger exchange interactions and smaller ligand field splittings⁵⁵.

The variation of the relative angle of rotation between the two Cp rings alters the symmetry of the metallocene. Thus, an eclipsed position corresponds to a D_{5h} symmetry, while a staggered position of the rings results in a D_{5d} symmetry. Although at low temperatures the relative orientation of the rings is closer to eclipsed, and D_{5h} is

usually a genuine minimum⁵⁶, the energy barrier of ring rotation is estimated⁵⁵ to be of about 1-2 kcal mol⁻¹. Although symmetry labels of the molecular orbitals change depending on the consideration of D_{5h} or D_{5d} symmetry, the essential details about structure and bonding are the same.

To accept a ligand the metallocene first bends and its frontier orbitals split as shown in Fig. 3.3. The a_{1g} orbital transforms into the 2a₁ orbital, mainly of d_{z²} character but with a small contribution of the s and d_{x²-y²} orbitals. The e_{2g} orbitals split, yielding a 1a₁ orbital, mainly formed by the d_{x²-y²} orbital (with a small contribution of the d_{z²} orbital) and a b₂ orbital of d_{xy} character. 2a₁ orbital increases its energy when bending, partly due to the avoided crossing with the 1a₁ orbital, and partly because of an increase in overlap with the π Cp orbitals. The 1a₁ orbital remains basically of the same energy due to the avoided crossing with 2a₁. The b₂ orbital rises in energy because it loses some overlap with the π* Cp orbitals. Since the frontier orbitals, with the exception of the 1a₁ orbital, increase their energy when the two Cp rings bent back, it is expected that the degree of bending decreases when adding d electrons, thus increasing the relative stability of the parallel disposition. As well, high spin species are expected to have a greater trend towards a geometry with parallel Cp rings than low spin species.

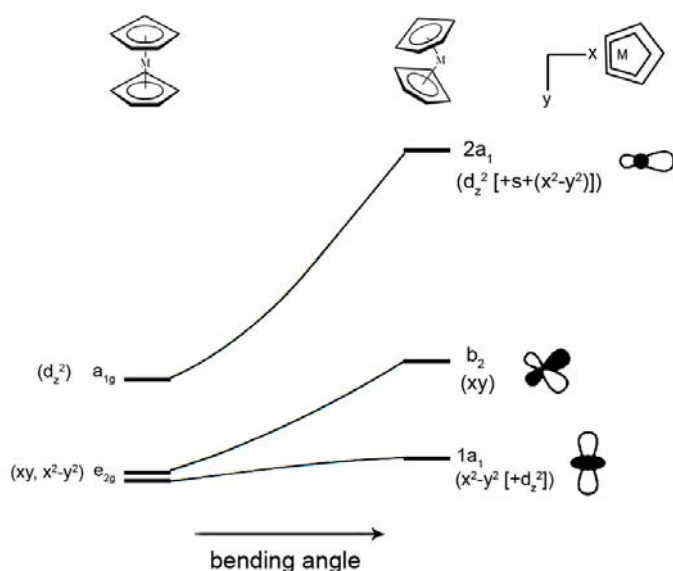


Fig. 3.3 Diagram representing the qualitative change in energy of the frontier molecular orbitals as the Cp rings bend back. The 2a₁, b₂ and 1a₁ orbitals are schematically represented, as seen from the z-axis perspective. They have a proper symmetry to accept as far as three additional ligands³.

The number of frontier orbitals involved in the bonding with additional ligands depends on the number of ligands and the number of empty orbitals in the metal, as shown in Fig. 3.4. There are no structurally characterized examples of metallocene molecules

bound to three monodentate ligands other than hydrogen⁵⁵. Cases in which three ligands are bound to the metallocene will not be considered in this work.

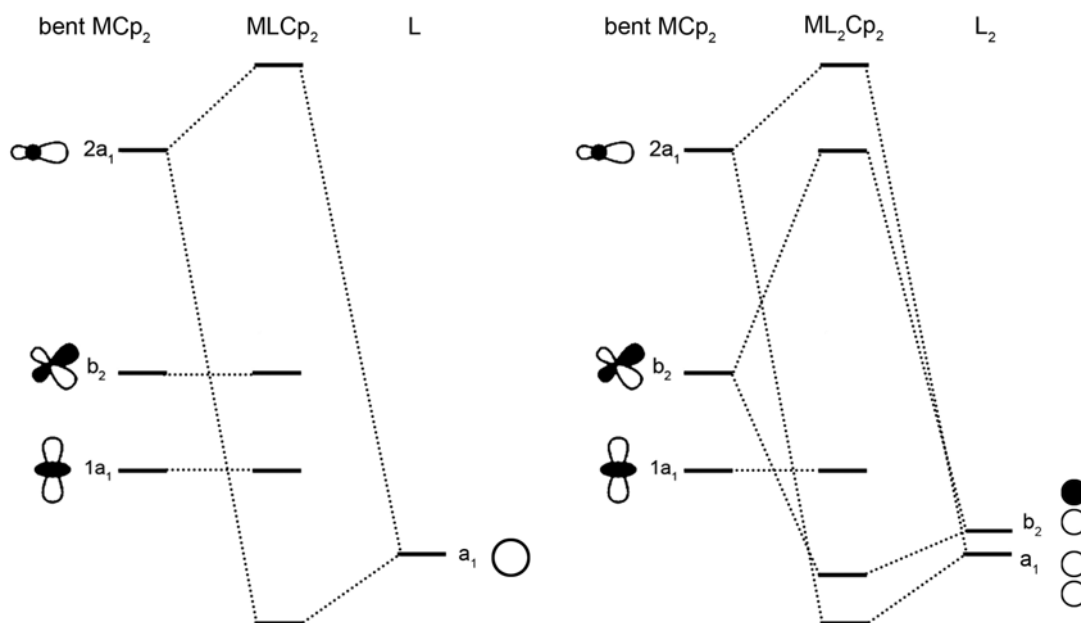


Fig. 3.4 Molecular orbital schemes for binding a bent metallocene unit to the s orbitals of one and two monodentate ligands, whose lineal combination results in two molecular orbitals of a₁ and b₂ symmetry. The 2a₁, b₂ and 1a₁ orbitals of the metallocene are the frontier orbitals.

When the ligands have π -donor character (such as the case of halogens), their p orbitals can interact with the empty π molecular orbitals of the metallocene. A metallocene fragment readily provides only one acceptor π orbital, the b₂ orbital shown in Figures 3.3 and 3.4, as long as it is empty. The d_{yz} orbital of the metal is involved in bonding to the Cp rings in the b₁ orbital, but its anti-bonding counterpart descends in energy on bending; although lies some 1.5 eV above the 2a₁ orbital⁵⁵ it could be considered as a fourth frontier orbital. Strong π -donors could effectively interact with the b₁* orbital weakening the bond of the metal with the Cp rings.

3.3. STRUCTURAL PARAMETERS OF METALLOCENES

Some useful structural parameters are usually defined to determine metallocene geometries⁵⁵. These are depicted in Fig. 3.5. In this work, though, the main geometric parameters that will be used will be angles γ and θ , as well as carbon-metal distances.

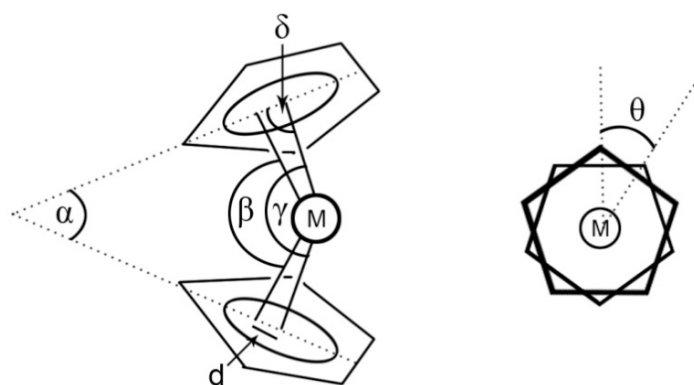


Fig. 3.5 α : Angle between the ring planes, β : Angle between the normals from the metal to the ring planes, γ : ring centroid-metal –ring centroid angle, δ : Angle between the metal ring and the metal-ring centroid vector, d : Displacement of the ring centroid from the normal to the ring plane, θ : Angle of rotation of the two rings (carbon-ring centroid-ring centroid-carbon dihedral angle).

3.4. USES AND RISKS OF THE SF₆⁵⁷

Sulfur hexafluoride is a colorless, odorless, tasteless and incombustible gas at normal conditions, widely used also in a variety of industrial processes, commercial products and scientific fields. However, SF₆ is one of the most potent greenhouse gases, with an estimated lifetime of 3,200 years in the atmosphere and a global warming potential of 22,450, and has been blanketed into the Kyoto protocol⁵⁸.

Due to its high dielectric strength and low toxicity, SF₆ is being used as an insulating gas in electronic and electrical equipment; as well as an etching gas, a blanketing gas for protecting molten aluminum or magnesium, and also as a tracer gas in ventilation efficiency. Sulfur hexafluoride is also used as an insulating gas in double pane sound-insulating windows, tires and soles of sport shoes; in retinal detachment repair operations, as a contract agent for ultrasound imaging and in several additional applications.

It has been noted although that, in spite of its inertness and of not representing a significant threat to human health, SF₆ can break down in a wide variety of species by electrical and thermal decomposition in the presence of other molecules, and its decomposition products are generally toxic. Two of the most toxic ones are SF₄ and S₂F₁₀, with occupational exposure limits of 0.1 and 0.01 ppm respectively⁵⁹⁻⁶¹.

SF₄, or sulfur tetrafluoride, is a nonflammable and colorless gas with an irritating odor, readily hydrolyzed by moisture forming hydrofluoric acid and thionyl fluoride. S₂F₁₀, disulfur decafluoride, is the dimer of the radical specie SF₅, sulfur pentafluoride, and is

a colorless volatile and insoluble in water liquid. It is hydrolyzed by water and alkalis, and at high temperatures disproportionates into SF₆ and SF₄.

In spite of its appreciated inertness and that it was not considered an established reagent, Ernst et al.^{62,63} report that “with low valent organometallic compounds, SF₆ can not only be quite reactive at and even below room temperature, serving as a useful and selective fluorinating agent, but also quite surprisingly, its reactivities can rival or exceed those of some commonly employed fluorinating agents”.

3.5. AN ALTERNATING DISSOCIATION ENERGY PATTERN⁶⁴

SF_n (n = 1-6) species bond dissociation energies do not follow a regular pattern. As outlined in Fig. 3.6, bond dissociation energies of neutral closed shell species that yield neutral species with unpaired electrons are larger than bond dissociation energies of neutral species with unpaired electrons that yield neutral closed shell species. For instance, the energy required to separate one fluorine atom from SF₆ is of 101.0 kcal mol⁻¹; while the energy required to separate a fluorine atom from the radical specie SF₅ is less than a half: 43.3 kcal mol⁻¹. The dissociation of one fluorine atom from SF₄ involves 96.3 kcal mol⁻¹, which is only slightly lower than the bond dissociation energy of SF₆. This can be understood by recognizing that molecular species with fully-filled 8 (SF₂), 10 (SF₄) and 12 (SF₆) valence electron shells around the S atom are more stable than other species. SF₆ has the largest bond dissociation energy so its S-F bond is the strongest one.

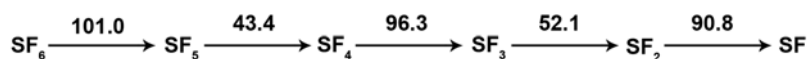


Fig. 3.6. Alternating bond dissociation experimental energies⁶⁴ for SF_n species, expressed in kcal mol⁻¹.

3.6. THE NATURE OF THE S-F BOND ON SF₆

The study of the geometry, the nature of the bonding, and the hypervalence in SF₆ and in general in SF_n species has been many times treated since Pauling introduced the concept of orbital hybridization in 1931⁶⁵. In regard to the octet theory of Lewis and Langmuir^{66, 67}, hypervalent compounds of the second and higher row non-metals, such as SF₆, require the postulate of an “expanded octet” and hybridization schemes involving d orbitals resulting in sp³d and sp³d² hybrid orbitals. However, the large energy gap between the 3p and 3d orbitals stands against those hybridization models, and in general d orbital hybridization is not accepted as an explanation to hypervalence. Pauling proposed ionic resonance forms only involving s and p orbitals to overcome this problem, and several other models were proposed by other authors.

The three center/four electron (3c/4e) model, illustrated in Fig. 3.6., was developed by Rundle and Pimentel^{68,69}, and is the prevailing theoretical model for hypervalency. This model can be understood in terms of the interaction of three collinear atoms: a central atom (sulfur in the case of SF₆) and two ligands (fluorine atoms for example). If one p orbital of the central atom combines with one p orbital of each one of the ligands, three molecular orbitals are obtained: an occupied bonding one, an occupied nonbonding one, with the electron density located over the ligand atoms, and an unoccupied anti-bonding one.

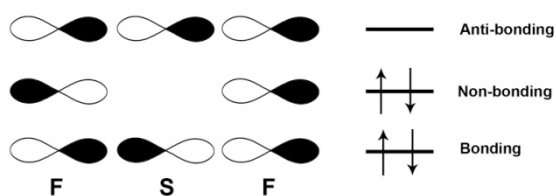


Fig. 3.6. Schematic representation of the 3c/4e model for an interaction involving three p orbitals and four electrons.

Woon and Dunning⁷⁰ have recently proposed a *recoupled pair bonding* model, which provides ready explanations for the oscillation of bond energies in the SF_n series, and the presence of low-lying excited states in SF and SF₂, as well as justifies the structures of the SF_n species. The primary statement of recoupled pair bonding is that hypervalence arises from the decoupling of a pair of electrons, which can be recoupled with other electrons to form new chemical bonds.

Reed and Weinbold⁷¹ studied the role of the d orbitals in SF₆ by ab initio methods. They pictured the electronic structure of SF₆ with a “zeroth-order” picture as a starting point consisting of an ionic model (F⁻ and S⁶⁺); a “first-order” picture, consisting of the transfer of about half an electron from the “p_σ” lone pair on each fluoride ion into the empty 3s and 3p orbitals of S⁶⁺; and a “second-order” picture, consisting of a charge transfer from the “p_σ” lone pairs of the fluorines into the sulfur “d_σ” orbitals of roughly 0.16 electrons, and a charge transfer from the “p_π” lone pairs of the fluorines into the sulfur “d_π” orbitals of roughly 0.09 electrons. Although the hypervalence bond can be represented just by the “first-order” picture, which employs only valence s and p functions, and central atom d hybridization is completely irrelevant to the nature of the chemical bonding in SF₆ due to a total 3d population of around 0.25 (being six times smaller than what would be necessary for a sp³d orbital hybridization with the 3d_σ orbitals), the influence of d orbitals should not be neglected, and studies lead to the conclusion that their inclusion could result in a more refined picture.

SF_n geometries can be qualitatively rationalized making use of the VSEPR theory⁵³. ¹SF₄, with four ligands and one non-bonding electron pair over the sulfur, has a trigonal bipyramid structure with the non-bonding electron pair filling an equatorial position. ²SF₅ has five ligands and one free electron, and has a structure of square-based pyramid; and ¹SF₆ has an octahedral geometry. This qualitative prediction is in accordance with calculated^{64,72,73} and experimental^{74,75} structures.

3.7. VANADOCENE FLUORINATION

As has been stated, S-F bond is not so inert in the presence of certain metallic compounds. The fact that this bond is significantly weaker than the C-F bond and many Metal-F bonds suggested that appropriate metallic reactants should be able to subtract one or more fluorine atoms from the sulfur via the equivalent of an inner-sphere electron-transfer process. The SF₆ reactions present one potential advantage: the products of the reaction are sulfur fluoride derivatives, which are more reactive than SF₆ and can react preferentially in successive fluorination reactions, ending up in a more efficient use of the available fluorine atoms and leading to sulfur rather than the highly

toxic SF₅ and SF₄ species. Furthermore, due to the inertness of SF₆ in normal conditions, it is a safer reactant than other more reactive fluorinating agents. The reaction experimentally carried out by Ernst et al.¹ could be roughly represented as in eq. 3.1:



Starting from this point, more possibilities could be considered. It may be that two fluorine atoms could coordinate with the vanadocene instead of one, yielding VCp₂F₂ and SF₄; or, after a first fluorination, a second one could take place in a second step, involving the same fluorinating molecule or another one; or, after the first fluorination, a V-S bond formation could take place, with subsequent α-elimination.

In this work though, and starting from the reaction in eq. 3.1, only the following reactions are studied due to time limitations:



In the next section a thermodynamic study of 3.2 and 3.3 will be done, and a kinetic study of 3.2. Although a kinetic study of 3.3 is not done for time reasons, future works should carry out with it.

4. PROCEDURE AND RESULTS

To represent the sets of molecular orbitals of the species involved, a 3-21G* basis set is used. This is a Pople's split-valence D-Z basis set⁷⁶⁻⁸¹ that describes each core electron with one atomic basis function (which is lineal combination of three Gaussian functions), and each valence electron with two atomic basis functions, one as a lineal combination of two Gaussian functions and the other constituted only by one Gaussian function. Moreover, 3-21G* basis set adds polarization functions but only to the second row elements. In our case then, only polarization functions to the sulfur atom will be added. 3-21G* is a small basis set that, in principle, allows to do qualitative predictions at a low computational cost. All the calculations have been performed with Gaussian03 package⁸² using DFT method and a B3LYP hybrid functional^{26,28,30}.

4.1. GEOMETRY AND ENERGY FOR ISOLATED SPECIES

As stated in the previous chapter, it is expected as much as a double fluorination of the vanadocene molecule, thus vanadocene, mono-fluorinated vanadocene and bi-fluorinated vanadocene must be considered. The possible fluorinating agents are the SF₆ and the derivatives generated from the loss of fluorine atoms -namely, SF₅, SF₄, SF₃, SF₂, and SF. In this work we will restrict the study only to SF₆, SF₅ and SF₄ for time reasons in spite that for a more complete study SF₃, SF₂ and SF should also be considered. The total energies and the energy differences between the low spin and high spin states of all the species are listed in table 4.1. High spin states for SF₆, SF₅ and SF₄ will not be considered

Table 4.1. Total energy values obtained for the vanadocene and SF_n species at the B3LYP/3-21G* level and energy differences between the high and low spin states. (Energy values are in atomic units).

	Total energy	ΔE
⁴ VCp ₂	-1324.488183	-39.8
² VCp ₂	-1324.424696	0.0
³ VFCp ₂	-1423.849164	-9.7
¹ VFCp ₂	-1423.833743	0.0
⁴ VF ₂ Cp ₂	-1523.144961	28.3
² VF ₂ Cp ₂	-1523.190075	0.0
³ SF ₆	-991.855287	141.1
¹ SF ₆	-992.080137	0.0
⁴ SF ₅	-892.568615	100.0
² SF ₅	-892.727486	0.0
³ SF ₄	-793.338573	82.9
¹ SF ₄	-793.470720	0.0

because of the large energy difference values obtained between the high and low spin states.

The minimum of the potential energy for each molecule is determined and confirmed with a frequencies calculation (results of frequencies calculations can be found in Table 4.3). A comparison of the energy values obtained for $^1\text{SF}_6$, $^2\text{SF}_5$ and $^1\text{SF}_4$ with experimental and theoretical values from other works is shown in Table 4.2. The obtained values at the B3LYP/3-21G* level are in quiet good accordance with the theoretical values obtained in other works with more expensive methods, as well as with experimental values. Those values are also in accordance with the alternating bond dissociation energy trends of the SF_n compounds. The dissociation energy to go from $^1\text{SF}_6$ to the radical compound $^2\text{SF}_5$ ($107.0 \text{ kcal mol}^{-1}$) is more than two times the dissociation energy to go from $^2\text{SF}_5$ to $^1\text{SF}_4$ ($46.8 \text{ kcal mol}^{-1}$). The structural parameters, shown in Fig. 4.1, are in good accordance with the experimental values too.

Table 4.2. Theoretical results for total energies and dissociation energies for $^1\text{SF}_6$, $^2\text{SF}_5$ and $^1\text{SF}_4$.

	Total energy ^a	Bond dissociation energy ^b
$^1\text{SF}_6$		
Present work	-992.080137	107.0
RCCSD(T)/AVQZ ^c		105.6
G2(MP2) ^d	-996.16457	106.9
G3 ^e	-996.79743	105.6
Exp. ^f		101.0 ± 3.4
$^2\text{SF}_5$		
Present work	-892.727486	46.8
RCCSD(T)/AVQZ ^c		39.2
G2/G2(MP2) ^d	-896.36530	38.1
G3 ^e	-896.94695	39.0
Exp. ^g		43.4 ± 6.0
$^1\text{SF}_4$		
Present work	-793.470720	
RCCSD(T)/AVQZ ^c		
G2/G2(MP2) ^d	-796.67566	
G3 ^e	-797.20226	

^aIn atomic units. ^b $\text{SF}_{n-1}\text{-F}$ dissociation energies in kcal/mol. ^cRef. 70, ^dRef. 64, ^eRef. 85. Dissociation energy data at 298K. ^fRef. 86. ^gRef. 87

For vanadocenes, as it is shown in Table 4.1, the high spin species $^4\text{VCp}_2$ and $^3\text{VFCp}_2$ have a lower energy than the low spin $^2\text{VCp}_2$ and $^1\text{VFCp}_2$ species. However, according to our calculations, the low spin $^2\text{VF}_2\text{Cp}_2$ is more stable than the high spin $^4\text{VF}_2\text{Cp}_2$, which at a first sight seems to go against the expected higher stability of the high spin complexes. This difference can be understood from the fact that, for the VF_2Cp_2 to acquire a quartet configuration, it is required that one electron fills an anti-bonding

orbital, high in energy. Fig. 4.2 shows that while ${}^2\text{VF}_2\text{Cp}_2$ has a η^5 hapticity for both Cp rings, ${}^4\text{VF}_2\text{Cp}_2$, has a η^5 hapticity for one Cp ring, but seems to have a η^2 hapticity for the other one.

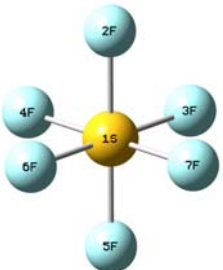
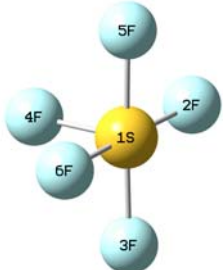
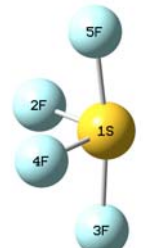
		a	b	c	Exp.
	d(S-F)	1.586	1.561	1.593	1.557 ^d
	$\alpha(\text{F-S-F})$	90.0	90.0	90.0	
	d(S-F _{2,3,5,6})	1.630	1.595	1.623	
	d(S-F ₄)	1.576	1.540	1.577	
	$\alpha(\text{F}_{2,3,5,6}\text{-S-F}_{2,3,5,6})$	90.0		90.0	
	$\alpha(\text{F}_{2,3,5,6}\text{-S-F}_4)$	91.2	91.6	91.4	
	d(S-F _{3,5})	1.655	1.645	1.663	1.646 ^e
	d(S-F _{2,4})	1.594	1.548	1.585	1.545 ^e
	$\alpha(\text{F}_3\text{-S-F}_5)$	171.7	172.1	171.1	173.1 ^e
	$\alpha(\text{F}_2\text{-S-F}_4)$	100.9	101.4	102.0	101.6 ^e
	$\alpha(\text{F}_{3,5}\text{-S-F}_{2,4})$	87.3	87.5	87.2	

Fig. 4.1. Structural parameters for ${}^1\text{SF}_6$, ${}^2\text{SF}_5$ and ${}^1\text{SF}_4$. All the distances are in Ångstroms, and the angles are in degrees.

^aThis work, ^b RCCSD(T)/AVQZ Ref. 70, ^cMP2=full/6-31G* Ref. 72, ^dRef. 83, ^eRef. 84

Fig. 4.3 shows the anti-bonding nature of the LUMO of ${}^2\text{VF}_2\text{Cp}_2$, with an anti-bonding interaction between the d_{xz} orbital of the vanadium and the π orbitals of the cyclopentadienyl rings. Experimental values for the structure of ${}^3\text{VFCp}_2$, shown in Fig. 4.2. are in qualitative agreement with the values obtained in this work. For some unknown reason the optimization of the low spin ${}^2\text{VCp}_2$ was more difficult. However, a bent structure, also shown in Fig. 4.2, is found after optimizing this molecule with a very tight convergence criterion. But a frequencies calculation (Table 4.3) shows that this structure does not belong to an absolute minimum since the smallest vibrational frequency has a negative value with respect to the angle orthogonal to the bending angle of the Cp rings. Due to time limitations and in spite of not being an absolute minimum

we have taken that shown in Fig. 4.2. as the minimum as all tests done did not give any lower energy structure. The bending angles of low spin electronic configurations for other metallocenes have been calculated to be smaller than 180 degrees⁵⁵. For the minimum of 4VCp_2 a parallel conformation of the Cp rings is obtained, which exemplifies how the occupation of the d orbitals controls the bending angle.

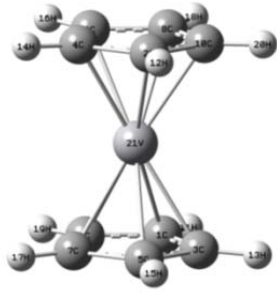
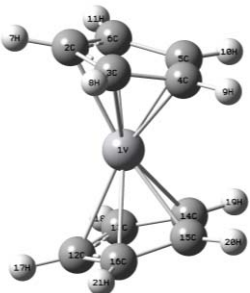
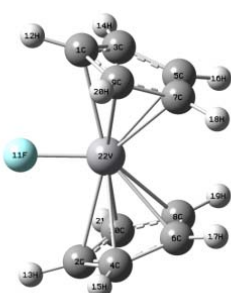
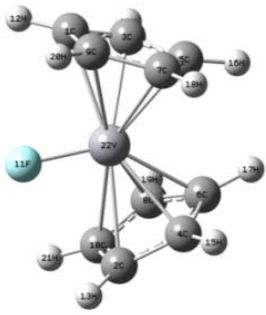
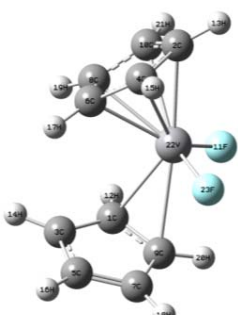
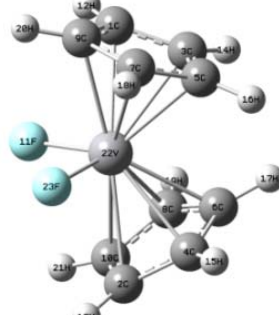
4VCp_2	2VCp_2	3VFCp_2			
					
Average d(V-C) Bending angle Cp rotation angle	2.281 180.0 0.0	Average d(V-C) Bending angle Cp rotation angle	2.200 165.2 0.0	Average d(V-C) d(V-F) Bending angle Cp rotation angle	2.336 (2.291) ^a 1.797 (1.913) ^a 145.2 (143.4) ^a 0.3
1VFCp_2	4VF_2Cp_2	2VF_2Cp_2			
					
Average d(V-C) d(V-F) Bending angle Cp rotation angle	2.290 1.767 143.5 0.4	Average d(V-η ⁵ Cp) Average d(V-η ² Cp) d(V-F ₁) d(V-F ₂) α(F-V-F)	2.330 2.475 1.768 1.778 106.8	Average d(V-Cp ₁) Average d(V-Cp ₂) d(V-F ₁) d(V-F ₂) α(F-V-F) Bending angle Cp rotation angle	2.355 2.361 1.797 1.797 86.2 133.9 38.9

Fig. 4.2. Geometries of the low and high spin VF_xCp_2 ($x = 0, 1, 2$) complexes at the B3LYP/3-21G* level. Experimental values are in parenthesis.

^aRef. 1

Table 4.3. Results of the frequencies calculations to evaluate the reliance of the calculated minima. The three lower frequency values are listed for each molecule. All the values are in cm^{-1} . Experimental values are in parenthesis.

$^1\text{SF}_6$	$^2\text{SF}_5$	$^1\text{SF}_4$	$^4\text{VCp}_2$
325.4 (347 ^a) 325.4 (347 ^a) 325.4 (347 ^a)	209.3 321.1 321.2	209.3 321.1 321.2	27.6 104.1 104.6
$^2\text{VCp}_2$	$^3\text{VFCp}_2$	$^1\text{VFCp}_2$	$^4\text{VF}_2\text{Cp}_2$
-41.6 62.5 101.6	10.6 52.5 167.5	33.2 80.8 165.4	39.4 45.9 82.9
$^2\text{VF}_2\text{Cp}_2$			
19.6 63.1 181.2			

^aRef. 89. ^bRef. 90 & 91.

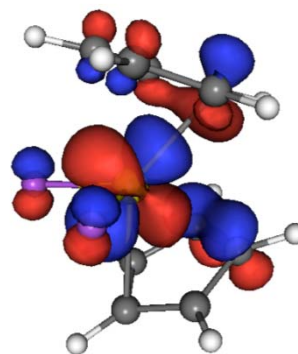


Fig. 4.6. LUMO of the $^2\text{VF}_2\text{Cp}_2$. Anti-bonding overlap can be appreciated between the ring π orbitals and the d_{xy} orbital of the vanadium.

The spin allowed reactions for the $\text{VCp}_2 + \text{SF}_6$ reaction are numbered from 4.1 to 4.6.

Electronic configurations of the frontier orbitals are shown also:

a) Mono-fluorination



b) Bi-fluorination



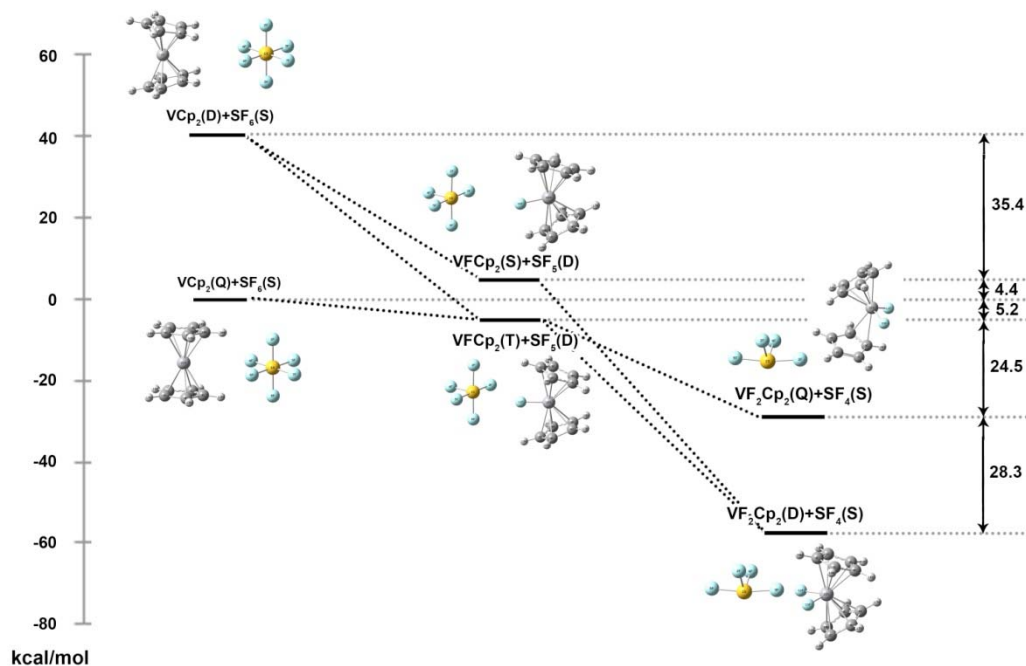
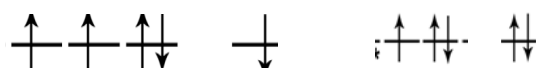


Fig. 4.4. Energy diagram showing the relative energies between the different steps considered. Each of the energies corresponds to the sum of the energies of two molecules calculated separately. The diagram also shows which reactions are spin-allowed connecting reactives and products through dotted lines. Relative zero energy is arbitrarily set on ${}^4\text{VCp}_2 + {}^1\text{SF}_6$.

4.2. THE MONO-FLUORINATION REACTION OF THE HIGH SPIN VANADOCENE

4.2.1. A THERMODYNAMIC PROFILE

Fig. 4.4 shows a diagram of energies of the isolated reactants and products for the first and second fluorination (reactions 3.1 and 3.2) for all spin states allowed. This can be done by adding the energy of the isolated interacting fragments. The minimum thermodynamic path is from the ${}^4\text{VCp}_2$ to the ${}^3\text{VFCp}_2$, and then to the ${}^2\text{VF}_2\text{Cp}_2$. A small stabilizing decrease in energy ($5.2 \text{ kcal mol}^{-1}$ at the B3LYP/3-21G* level) exists for the

first fluorination, and a larger decrease (52.8 kcal mol⁻¹) is calculated when going from the mono-fluorinated vanadocene to the bi-fluorinated vanadocene.

A better view can be obtained by looking at the interaction energy of the interacting fragments (that is, the cluster molecule 1 + molecule 2). For a detailed study of one of the reactions involved in the whole map, the mono-fluorination reaction of the high spin ⁴VCp₂, the supramolecular structures involving the molecules conforming reactives and the molecules conforming products, respectively, at a close distance need to be calculated. Supramolecules will be designed indicating the total multiplicity, as well as the multiplicity of each molecule to avoid ambiguity. To obtain the supramolecule of the reactives, ⁴(⁴VCp₂-¹SF₆), the two optimized geometries are simply put together and optimized. The same procedure is followed to find the supramolecule of products, ⁴(³VFCp₂-²SF₅). The energy minima have been confirmed with frequencies calculations (see Table 4.5). The charge distribution and the spin density of the supramolecules obtained are nearly equivalent to the charge distribution and the spin density of the separated species and in any case no remarkable differences arise (Mulliken atomic charges and Mulliken spin density populations for isolated molecules and supramolecules are compared in appendices A2).

The optimum geometries of these aggregates, shown in Table 4.4, when compared to those for the isolated species of Figures 4.1 and 4.2, they present some slight differences. The most notable may be the variation of the relative rotation angle of the Cp rings in the case of ³VFCp₂. In the isolated specie, that angle has a value of nearly 0° (0.3°), i.e. the rings are eclipsed; while in the supramolecule ⁴(³VFCp₂-²SF₅) it has a value of 31.7°, which corresponds to a nearly staggered ring conformation. The staggered conformation allows one of the two axial fluorine atoms to be at an appropriate H...F interaction distance of two hydrogen atoms (2.425 and 2.461 Å respectively), thus maximizing the number of H...F stabilizing interactions, while in the eclipsed conformation only one H...F interaction can be properly established by each of the axial fluorine atoms. For H...F interactions in crystals involving neutral species, where the hydrogen atom is bound to a carbon atom, distances H-F have been found to range from 2.320 Å to 2.912 Å⁸⁸.

The barrier estimated for the rotation of the two Cp rings at the B3LYP/3-21G* level (see Appendices A3) is about 0.2 kcal mol⁻¹. A very low value –one order of magnitude lower than the estimated value of 1-2 kcal mol⁻¹ on Ref. 57- which readily allows us to suppose that a free rotation of the Cp rings is permitted.

Table 4.4. Geometries of the ⁴(⁴VCp₂-¹SF₆) and ⁴(³VFCp₂-²SF₅) supramolecules. Distances are expressed in Angstroms, angles are expressed in degrees.

⁴ (VCp ₂ -SF ₆)	⁴ (VFCp ₂ -SF ₅)																																																																														
<table border="0"> <tr><td>Average d(V-Cp)</td><td>2.282</td></tr> <tr><td>Average d(V-Cp')</td><td>2.282</td></tr> <tr><td>Cp bending angle</td><td>175.2</td></tr> <tr><td>Cp rotation angle</td><td>-0.6</td></tr> <tr><td>d(V-F₂₂)</td><td>3.506</td></tr> <tr><td>d(V-F₂₄)</td><td>3.498</td></tr> <tr><td>d(S-F₂₂)</td><td>1.592</td></tr> <tr><td>d(S-F₂₄)</td><td>1.593</td></tr> <tr><td>Average d(S-F_{26,27})</td><td>1.594</td></tr> <tr><td>Average d(S-F_{25,28})</td><td>1.584</td></tr> <tr><td>α (F₂₆-S-F₂₇)</td><td>179.2</td></tr> <tr><td>α (F₂₂-S-F₂₄)</td><td>89.8</td></tr> <tr><td>α (F₂₅-S-F₂₈)</td><td>90.4</td></tr> <tr><td>d(F₂₆-H₁₁)</td><td>2.272</td></tr> <tr><td>d(F₂₇-H₁₈)</td><td>2.273</td></tr> <tr><td>Average d(F₂₂-H_{11,18})</td><td>2.591</td></tr> <tr><td>Average d(F₂₄-H_{11,18})</td><td>2.590</td></tr> </table>	Average d(V-Cp)	2.282	Average d(V-Cp')	2.282	Cp bending angle	175.2	Cp rotation angle	-0.6	d(V-F ₂₂)	3.506	d(V-F ₂₄)	3.498	d(S-F ₂₂)	1.592	d(S-F ₂₄)	1.593	Average d(S-F _{26,27})	1.594	Average d(S-F _{25,28})	1.584	α (F ₂₆ -S-F ₂₇)	179.2	α (F ₂₂ -S-F ₂₄)	89.8	α (F ₂₅ -S-F ₂₈)	90.4	d(F ₂₆ -H ₁₁)	2.272	d(F ₂₇ -H ₁₈)	2.273	Average d(F ₂₂ -H _{11,18})	2.591	Average d(F ₂₄ -H _{11,18})	2.590	<table border="0"> <tr><td>Average d(V-Cp)</td><td>2.318</td></tr> <tr><td>Average d(V-Cp')</td><td>2.316</td></tr> <tr><td>Cp bending angle</td><td>143.9</td></tr> <tr><td>Cp rotation angle</td><td>31.7</td></tr> <tr><td>d(V-F₂₂)</td><td>1.902</td></tr> <tr><td>d(V-F₂₄)</td><td>2.807</td></tr> <tr><td>d(S-F₂₂)</td><td>2.245</td></tr> <tr><td>d(S-F₂₄)</td><td>1.710</td></tr> <tr><td>Average d(S-F_{26,27})</td><td>1.664</td></tr> <tr><td>Average d(S-F_{25,28})</td><td>1.609</td></tr> <tr><td>α (F₂₆-S-F₂₇)</td><td>178.3</td></tr> <tr><td>d(S-F₂₈)</td><td>1.586</td></tr> <tr><td>Average d(S-F_{24,25,26,27})</td><td>1.667</td></tr> <tr><td>Average α (F₂₈-S-F_{24,25,26,27})</td><td>90.0</td></tr> <tr><td>Average α (F_{24,25,26,27}-S-F_{24,25,26,37})</td><td>90.0</td></tr> <tr><td>d(F₂₇-H₁₈)</td><td>2.415</td></tr> <tr><td>d(F₂₇-H₂₀)</td><td>2.461</td></tr> <tr><td>d(F₂₆-H₁₁)</td><td>2.185</td></tr> <tr><td>d(F₂₄-H₂₀)</td><td>2.525</td></tr> <tr><td>d(F₂₄-H₁₁)</td><td>2.727</td></tr> <tr><td>d(F₂₂-H₁₈)</td><td>2.616</td></tr> <tr><td>d(F₂₂-H₁₁)</td><td>2.766</td></tr> </table>	Average d(V-Cp)	2.318	Average d(V-Cp')	2.316	Cp bending angle	143.9	Cp rotation angle	31.7	d(V-F ₂₂)	1.902	d(V-F ₂₄)	2.807	d(S-F ₂₂)	2.245	d(S-F ₂₄)	1.710	Average d(S-F _{26,27})	1.664	Average d(S-F _{25,28})	1.609	α (F ₂₆ -S-F ₂₇)	178.3	d(S-F ₂₈)	1.586	Average d(S-F _{24,25,26,27})	1.667	Average α (F ₂₈ -S-F _{24,25,26,27})	90.0	Average α (F _{24,25,26,27} -S-F _{24,25,26,37})	90.0	d(F ₂₇ -H ₁₈)	2.415	d(F ₂₇ -H ₂₀)	2.461	d(F ₂₆ -H ₁₁)	2.185	d(F ₂₄ -H ₂₀)	2.525	d(F ₂₄ -H ₁₁)	2.727	d(F ₂₂ -H ₁₈)	2.616	d(F ₂₂ -H ₁₁)	2.766
Average d(V-Cp)	2.282																																																																														
Average d(V-Cp')	2.282																																																																														
Cp bending angle	175.2																																																																														
Cp rotation angle	-0.6																																																																														
d(V-F ₂₂)	3.506																																																																														
d(V-F ₂₄)	3.498																																																																														
d(S-F ₂₂)	1.592																																																																														
d(S-F ₂₄)	1.593																																																																														
Average d(S-F _{26,27})	1.594																																																																														
Average d(S-F _{25,28})	1.584																																																																														
α (F ₂₆ -S-F ₂₇)	179.2																																																																														
α (F ₂₂ -S-F ₂₄)	89.8																																																																														
α (F ₂₅ -S-F ₂₈)	90.4																																																																														
d(F ₂₆ -H ₁₁)	2.272																																																																														
d(F ₂₇ -H ₁₈)	2.273																																																																														
Average d(F ₂₂ -H _{11,18})	2.591																																																																														
Average d(F ₂₄ -H _{11,18})	2.590																																																																														
Average d(V-Cp)	2.318																																																																														
Average d(V-Cp')	2.316																																																																														
Cp bending angle	143.9																																																																														
Cp rotation angle	31.7																																																																														
d(V-F ₂₂)	1.902																																																																														
d(V-F ₂₄)	2.807																																																																														
d(S-F ₂₂)	2.245																																																																														
d(S-F ₂₄)	1.710																																																																														
Average d(S-F _{26,27})	1.664																																																																														
Average d(S-F _{25,28})	1.609																																																																														
α (F ₂₆ -S-F ₂₇)	178.3																																																																														
d(S-F ₂₈)	1.586																																																																														
Average d(S-F _{24,25,26,27})	1.667																																																																														
Average α (F ₂₈ -S-F _{24,25,26,27})	90.0																																																																														
Average α (F _{24,25,26,27} -S-F _{24,25,26,37})	90.0																																																																														
d(F ₂₇ -H ₁₈)	2.415																																																																														
d(F ₂₇ -H ₂₀)	2.461																																																																														
d(F ₂₆ -H ₁₁)	2.185																																																																														
d(F ₂₄ -H ₂₀)	2.525																																																																														
d(F ₂₄ -H ₁₁)	2.727																																																																														
d(F ₂₂ -H ₁₈)	2.616																																																																														
d(F ₂₂ -H ₁₁)	2.766																																																																														
E = -2316.587531 a. u.	E = -2316.628637 a. u.																																																																														

The heat of formation ($\Delta E_{f,SUP,R}$) for the formation of the supramolecules at the B3LYP/3-21G* level is of 12.0 kcal mol⁻¹, {calculated as $E(^1SF_6) + E(^4VCp_2) - E[^4(^4VCp_2-^1SF_6)]$ }, and 32.6 kcal mol⁻¹ for products { $E(^2SF_5) + E(^3VFCp_2) - E[^4(^3VFCp_2-^2SF_5)]$ }. As a consequence the aggregate for the products is more stable than that for the reactants (by 25.8 kcal mol⁻¹). Those energies are represented in Fig. 4.5., together with those of the isolated fragments. The $\Delta E_{f,SUP,P}$ for the supramolecule

Table 4.5. Results of the frequencies calculations to evaluate the reliance of the calculated minima. The three lower frequency values are listed for each molecule. All the values are in cm^{-1} . Experimental values are in parenthesis.

${}^4({}^4\text{VCp}_2\text{-}^1\text{SF}_6)$	${}^4({}^3\text{VFCp}_2\text{-}^2\text{SF}_5)$
19.6	35.3
27.5	56.5
56.8	77.9

of products is more than two times those found for the reactives and can be hardly explained by $\text{H}\cdots\text{F}$ interactions alone.

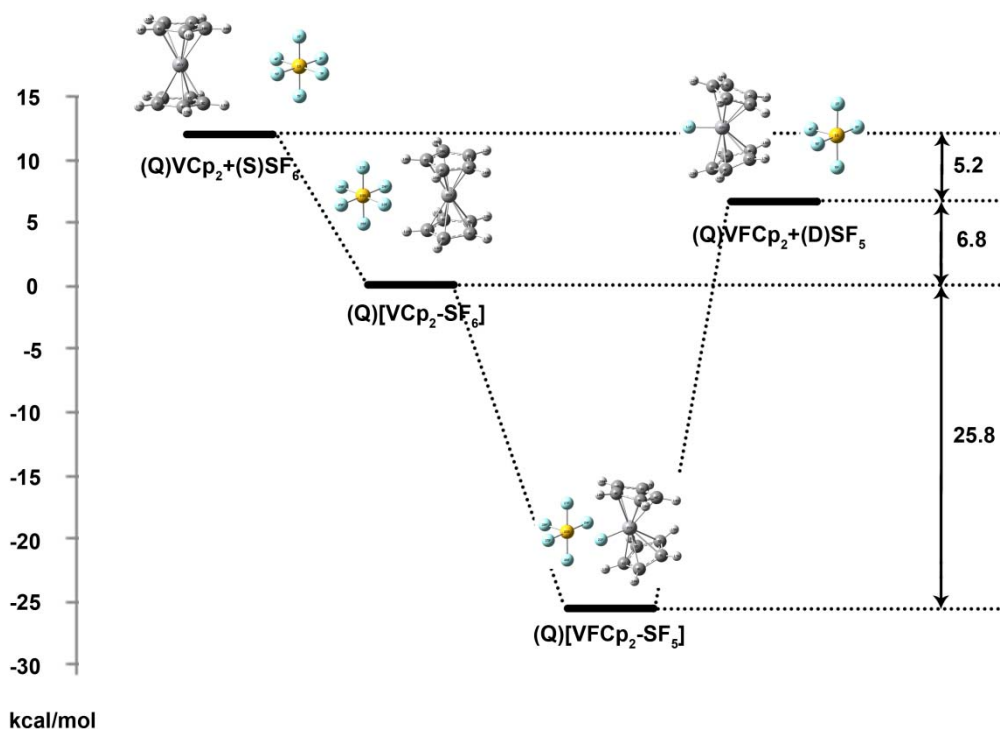


Fig. 4.5. Energy diagram for the monofluorination reaction of ${}^4\text{VCp}_2$ with ${}^1\text{SF}_6$. ${}^4\text{VCp}_2+{}^1\text{SF}_6$ are the reactives calculated separately; ${}^4(\text{VCp}_2\text{-SF}_6)$ represents the supramolecule of reactives. ${}^3\text{VFCp}_2+{}^2\text{SF}_5$ are the separate products; while ${}^4(\text{VFCp}_2+\text{SF}_5)$ accounts for the supramolecule of products. The zero of the scale is arbitrarily placed in reactants aggregate.

In order to confirm the validity of the $\Delta E_{f,\text{SUP,R}}$ and $\Delta E_{f,\text{SUP,P}}$, a set of calculations fixing different S-F distances and optimizing each geometry is performed on the ${}^4({}^4\text{VCp}_2\text{-}^1\text{SF}_6)$ aggregate (Fig. 4.6). An equivalent procedure for the supramolecule of products yields the curve in Fig. 4.7. From the geometries obtained (see Appendices A4) it is possible to observe that the SF_6 moves away from the VCp_2 molecule keeping as many $\text{F}\cdots\text{H}$

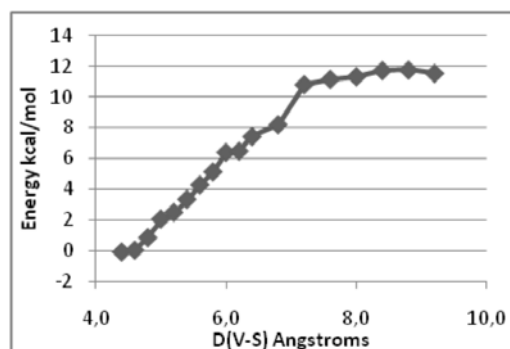


Fig. 4.6. Interaction energy curve for the supramolecule of reactives as a function of the V...S distance. The geometry was optimized on each point. The curve exhibits a nearly linear trend from 4.4 to 7.2 Å. The energy increases as the SF_6 moves away from the VCp_2 , until it reaches a constant value in which the two molecules are too far apart to interact.

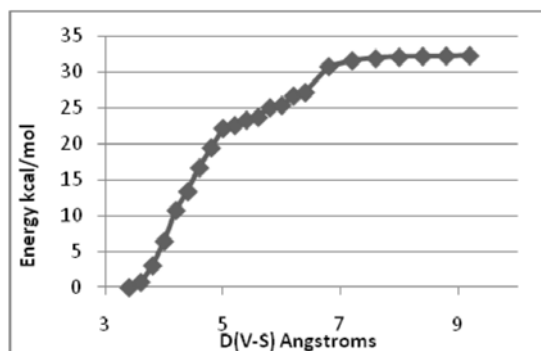


Fig. 4.7. Interaction energy curve for the supramolecule of products as a function of the V...S distance. Two different slopes can be identified: A fast increase from 3.2 to 5.0 Å, and a more moderate increase from 5.0 to around 7.0 Å. From 7.0 Å and on the energy becomes approximately constant.

interactions as possible. Even at relatively long S-V distances, H...F interactions between the fluorine atoms of the SF₆ and the protruding hydrogen atoms of the Cp rings are established. The H...F interactions in the supramolecule can justify a stabilisation of 12.0 kcal/mol in reactants.

However, the H...F interactions present in the products supramolecule alone

hardly account for the 32.6 kcal mol⁻¹ involved in the separation of the ²SF₅ and the ³VFCp₂. The remaining stabilizing contribution to the energy comes from a dipole-dipole interaction between the two molecules. As shown in Fig. 4.8, a permanent dipole moment exists in the SF₅ and VFCp₂ species. In the supramolecule ⁴(³VFCp₂-²SF₅) the two dipoles orient themselves in order to stabilize the system.

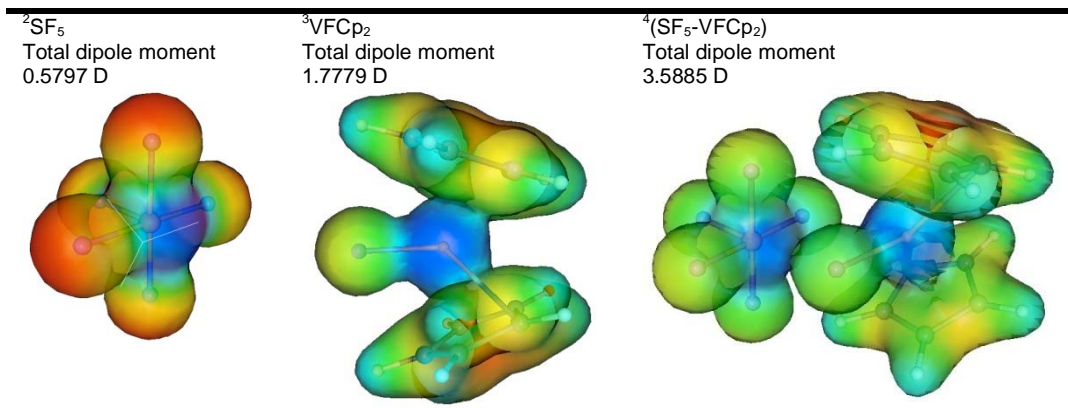


Fig. 4.8. Electron density and values of dipole moment for ²SF₅, ³VFCp₂ and ⁴(SF₅-VFCp₂).

4.2.2. A KINETIC PROFILE I. POTENTIAL ENERGY CURVE

To determine the kinetics of the F addition to VCp₂ from SF₆ one has to locate the transition state of the reaction of the transference. For that purpose, a potential energy curve was calculated, taking as a reaction coordinate the distance between the sulfur atom and the fluorine that is transferred to the vanadium. Along the reaction path, a sulfur-fluorine bond is broken, a vanadium-fluorine bond is formed and the Cp rings

bent. The first choice as reaction coordinate is the S-F distance. The V-F distance could be also selected. Two starting points could be taken to compute the curve: From reactives (Fig. 4.9) and from products (Fig. 4.10). In both cases, there is a large discontinuity in the zone supposedly close to the transition state, in which one would expect to find a maximum, with a sudden change in geometry: When going from reactives to products, at a S-F distance of 1.78 Å, the structure resembles that of reactives, with parallel rings. Elongating the distance in 0.01 Å causes a sudden bending and a big step on energy appears.

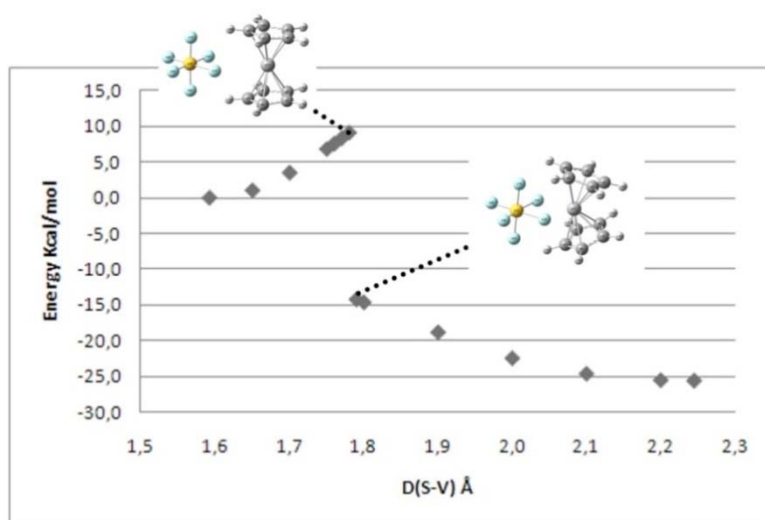


Fig. 4.9. Potential energy curve, calculated starting from the supramolecule of reactives. An abrupt step can be seen with a sudden change in geometry, and no smooth barrier allowing to obtain a reasonable initial geometry for the transition state optimization is found. The geometries corresponding to the two sides of the step are displayed. For energy values see Appendices A5.

For the products supramolecule, whose curve is represented in Fig. 4.10, through the same energy step is appreciated, there is an additional consideration: When, in the supramolecule ${}^4({}^3\text{VFCp}_2\text{-}^2\text{SF}_5)$, one fluorine atom moves away from vanadium to bind to sulfur, the neighboring fluorine atom tends to form a new bond with the vanadium atom, which supports the fact that the V-F bond is more stable than the S-F bond and the reaction is thermodynamically favorable. That means that for calculating the potential energy curve from products to reactives some restriction has to be done, either fixing the distance S-F or the distance V-F. The zone of the curve near to the reactives in Fig. 4.10 is then calculated fixing the distance from the sulfur atom to the fluorine that is transferred at different lengths, while the distance between the sulfur atom and the second fluorine nearest to the vanadium is maintained fixed at 1.631 Å. A step in

the energy around a distance S-F of 1.6-1.65 Å is appreciated, and it is remarkably differently located than the step found on the curve of Fig. 4.9 from reactives to products, around a S-F distance of 1.8 Å. The sudden change in the bending angle of the two Cp rings is also noticeable: The two Cp rings keep a bent conformation nearly untouched when decreasing the F-S distance, but once the energy step takes place, the bending angle is suddenly increased and the Cp rings adopt a nearly parallel conformation.

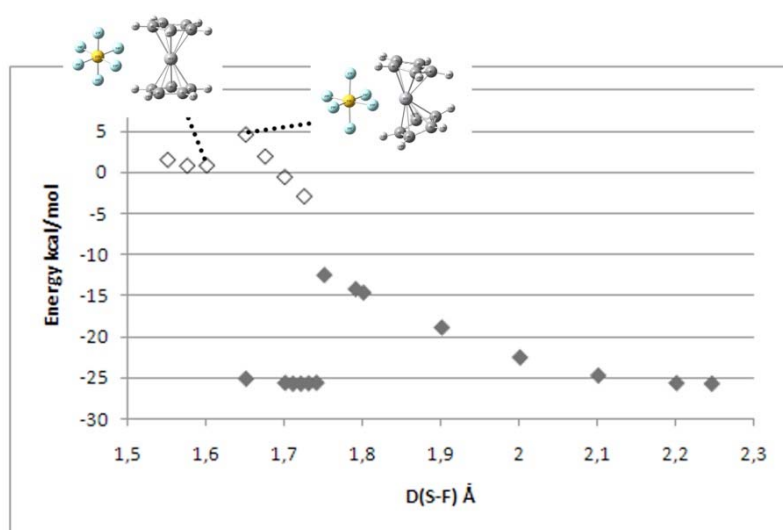


Fig. 4.10. Potential energy curve, calculated starting from the products supramolecule. Black points are calculated fixing only the S-F distance. Empty points are calculated fixing the distance between the sulfur and the second nearest to vanadium fluorine atom to 1.631 Å. The geometries corresponding to the two sides of the step are displayed. For energy values see Appendices A5.

4.2.3. A KINETIC PROFILE II. POTENTIAL ENERGY SURFACE

The potential energy curve built with the S-F distance as the only reaction coordinate does not allow to define a starting geometry for locating the transition state (Fig. 4.9 and 4.10), this suggests that other coordinates are important to define that transition state. Another potential energy curve built taking the bending angle as the main reaction coordinate gave results similar to those shown in Fig. 4.9 and 4.10 (see Appendices A6).

To overcome the problem of finding a starting geometry from which determine the transition state, a potential energy surface is built taking as reaction coordinates the V-F distance and the bending angle, fixing these parameters to different values and optimizing the geometry in each point.

4.2.3.1. DESIGN OF THE Z-MATRIX

To properly control the bending angle and the vanadium-fluorine distances the geometry must be expressed as a z-matrix built in a specific way. 16 dummy atoms are introduced and several constraints are required too. One dummy atom is located at the centroid of each ring, and the distances from the carbon atoms to its centroid are imposed to be equivalent, restricting the Cp rings to be regular pentagons. The angle formed by the carbon atoms of the Cp rings, the dummy in the center of that ring and the vanadium atom is imposed to be of 90° ; two dummies are attached also to the vanadium, forming a 90° angle in between, to control the two orthogonal angles that exist between the two dummies located at the ring centroids and the vanadium. To properly control the bending angle of the VCp₂ molecule, one of those orthogonal angles must be constrained to be of 90° , while the other acts as the bending angle. The vanadium to fluorine distances are well defined within the z-matrix, both for the fluorine that is being transferred as well as for the second nearest fluorine to the vanadium atom. This is done in order to avoid that, for long fluorine-vanadium distances and bent geometries, the second fluorine atom closer to vanadium spontaneously binds to the vanadium atom (this is the same effect already observed in the curve of fig. 3.10). For a few geometries (i.e. some of those where the Cp rings are very bent back -120°), in fact all the fluorine-vanadium distances must be fixed to avoid the bonding of an undesired fluorine atom to the vanadium. A more detailed explanation for the constraints as well as an example for this z-matrix are found in section A7 of the Appendices.

4.2.3.2. BUILDING THE POTENTIAL ENERGY SURFACE

Once the z-matrix is constructed and tested so that it can effectively represent both the geometry and energy of reactives and products, for the matter of building the surface a

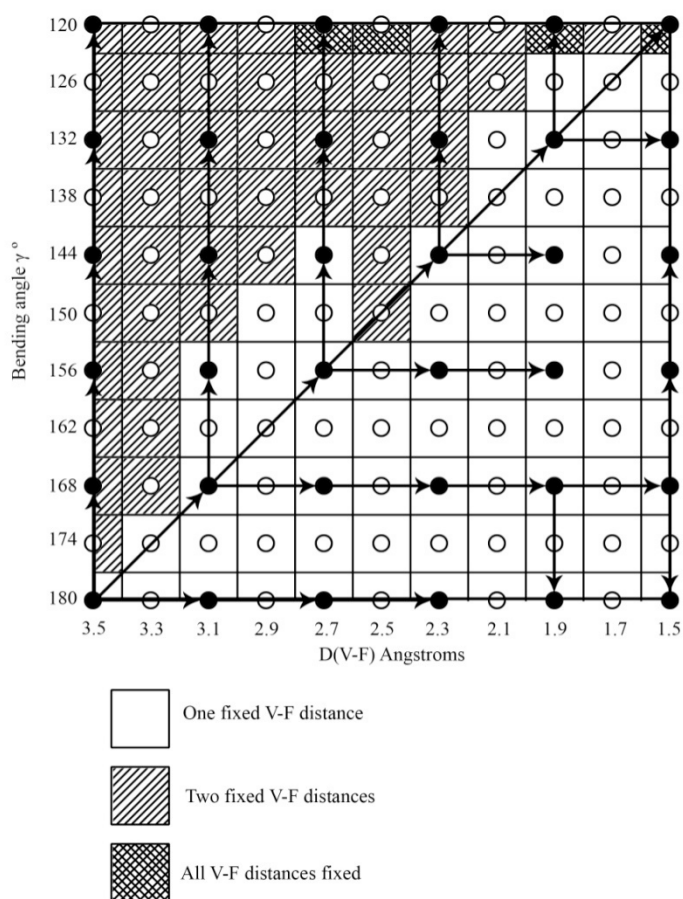


Fig. 4.11. Schematic grid showing the general procedure followed to calculate the potential energy surface. Black points represent the geometries that were optimized in a first calculation of the surface, and the arrows connecting them show the order in which were calculated and which point was used as initial geometry in each case. Empty points were calculated after all the black points were calculated, to make the surface look finer.

pretty simple procedure is followed: For the initial geometry, a fixed V-F distance of 3.5 Å and a fixed bending angle γ of 180° are taken (which represents a structure similar to the structure of the reactives) and the supramolecule is optimized with those constraints. This optimized structure is utilized to optimize three more points: (3.5 Å; 168°), (3.1 Å; 180°) and (3.1 Å; 168°), with 0.4 Å steps for the distance and 12° steps for the angle. Fig. 4.11 summarizes the order in which the points of the surface have been calculated, as well as the

geometrical restrictions involving each of them. In nearly half of the points the distance from the vanadium to the second nearest fluorine atom must be fixed too to avoid the formation of an undesired V-F bond. That restriction is applied in general where V-F distances are large and bending angles are small. After a first set of calculations, a second set of calculations with a 0.2 Å step for the V-F distance and a 6° step for the γ angle is performed utilizing the geometries of the points already obtained, to increase the resolution of the surface.

Two views of the potential energy surface obtained are shown in fig. 4.16, a low barrier is observed separating reactives and products. In both the zones of reactives and products, the surfaces are fairly smooth. To go from reactives to products a simultaneous shortening of the V-F distance and a bending of the Cp rings is required. This explains the discontinuity observed in the potential energy curves shown in Figures 4.9 and 4.10.

The absolute minimum of the potential energy surface corresponds to the point (1.9 Å; 144°) –while the respective coordinates for the energy minimum of the supramolecule of products are 1.902 Å and 143.9°. The energy difference between the true B3LYP/3-21G* theoretical minimum and the value obtained from the potential energy surface, calculated as $\{E[{}^4({}^3\text{VFCp}_2\text{-}^2\text{SF}_5)_{(1.9;144)}] - E[{}^4({}^3\text{VFCp}_2\text{-}^2\text{SF}_5)_{\text{min}}]\}$ is of 0.3 kcal mol⁻¹. The minimum value of the surface around the zone of reactives corresponds to the point (3.3 Å; 174°) while the respective values for the true B3LYP/3-21G* theoretical minimum of the supramolecule of reactives are 3.06 Å and 175.2° and the energy difference calculated as $\{E[{}^4({}^4\text{VCp}_2\text{-}^1\text{SF}_6)_{(3.3;174)}] - E[{}^4({}^4\text{VCp}_2\text{-}^1\text{SF}_6)_{\text{min}}]\}$ is of 0.04 kcal mol⁻¹, a negligible value. The structures obtained from the surface calculations represent very well the optimized structures corresponding to the minima.

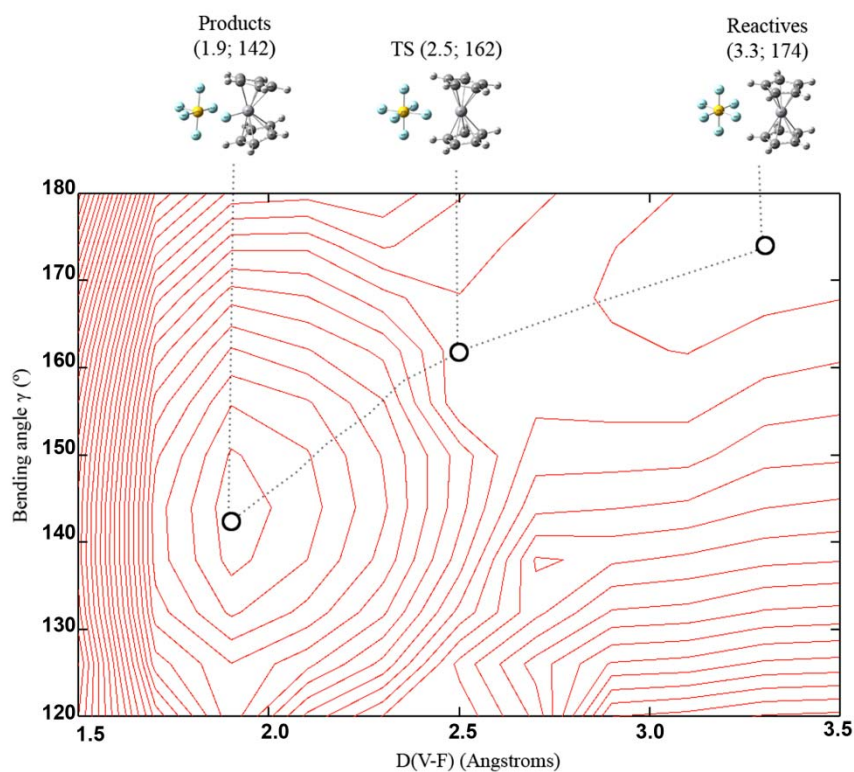
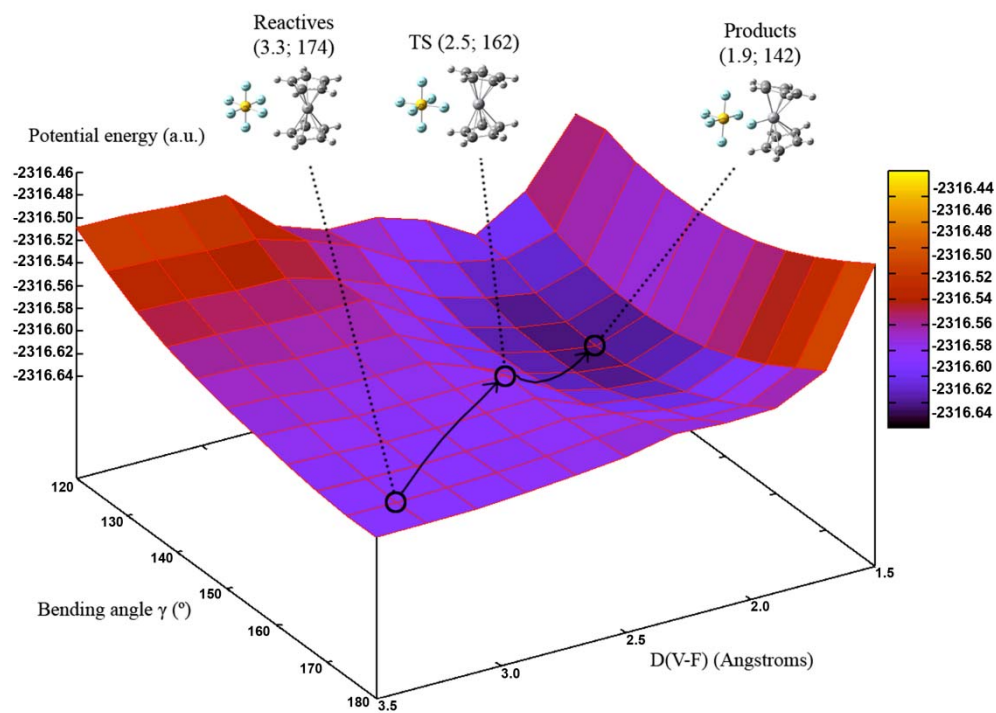


Fig. 4.12. Relaxed potential energy surface for the transference of one fluorine atom from ${}^1\text{SF}_6$ to ${}^4\text{VCP}_2$ to yield ${}^2\text{SF}_5$ and ${}^3\text{VFCP}_2$. The points nearest to reactives, products and the hypothetical transition state and their coordinates are shown in parentheses (V-F distance in Å; bending angle γ in degrees).

4.2.3.3. LOCATING THE TRANSITION STATE

For finding the transition state, the point (2.5 Å; 162°) is chosen as an initial starting point (Fig. 4.12). The geometry constraints are no longer imposed and the supramolecule is optimized using redundant internal coordinates, evaluating the Hessian in each point of the optimization and making use of extremely tight optimization convergence criteria.

The structure computed for the transition state is shown in Fig. 4.13, It has a total energy of -2316.581131 atomic units. The nature of the optimized structure is evaluated with a frequencies calculation and one imaginary frequency –being all the others real- is obtained. The mode associated with the negative frequency, whose value is -309.7382 cm^{-1} , corresponds to the transference of one fluorine atom from the sulfur to the vanadium, as shown in figure 4.14.

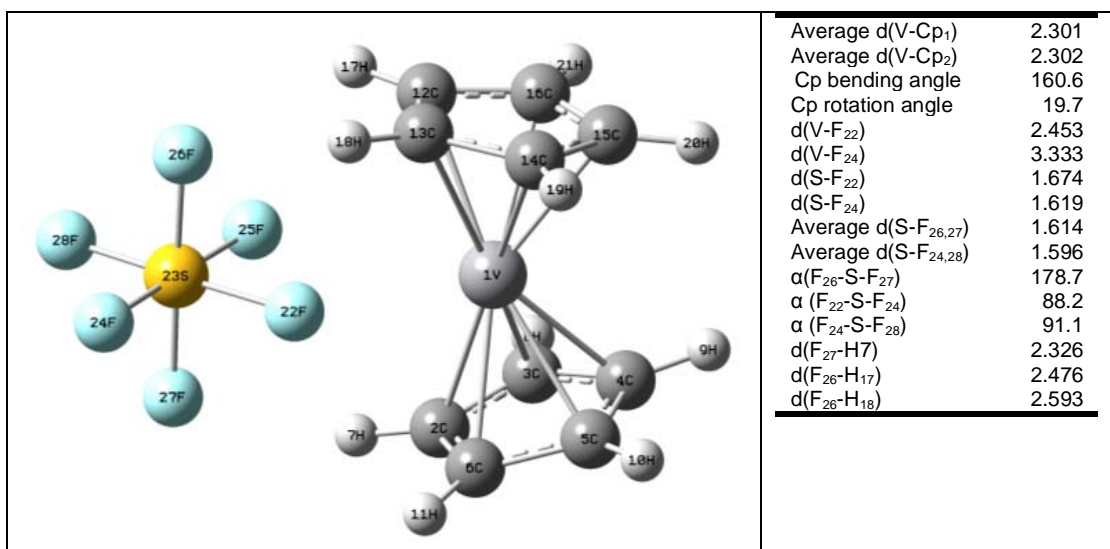


Fig. 4.13. Transition state geometry obtained at the B3LYP/3-21G* level. Distances are expressed in Angstroms, angles are expressed in degrees.

The structure of the transition state shows intermediate values for the distances and angles that range between the values of the reactives and the products. However, H...F distances are longer than in supramolecules of both reactives and products.

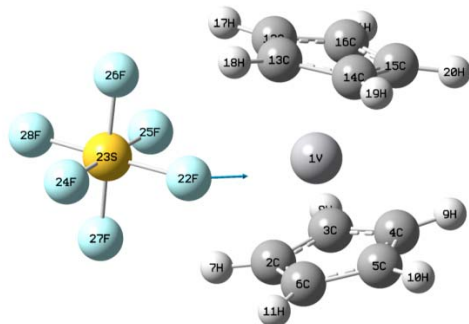


Fig. 4.14. Representation of the negative eigenvalue of the Hessian for the transition state structure found at B3LYP/3-21G* level. The displacement corresponds to the motion of the fluorine atom towards the vanadium atom.

4.2.4. POTENTIAL ENERGY DIAGRAM FOR THE MONO-FLUORINATION REACTION AT THE 3-21G* LEVEL

Figure 4.15 shows how the transition state found generates a low energy barrier for the mono-fluorination. The height of the barrier from the reactives supramolecule is of 4.0 kcal mol⁻¹, and from the products supramolecule is of 29.8 kcal mol⁻¹. In a general overview of the reaction, the isolated reactives ⁴VCp₂ and ¹SF₆ meet and form the supramolecule ⁴(⁴VCp₂-¹SF₆), stabilized by intermolecular H...F bonds (specifically between the axial fluorine atoms and the two hydrogens of the Cp rings facing the SF₆ molecule) that lower the energy in 12 kcal mol⁻¹, while two equatorial fluorines face the vanadium atom. From this geometry, the system can readily transfer one fluorine atom from the sulfur to the vanadium. The reaction involves a barrier of 4.0 kcal mol⁻¹. The analysis of the frontier orbitals of the transition state shows the set of three d-mixed orbitals of a₁ and b₂ symmetry expected for a bent vanadocene (Fig. 4.16).

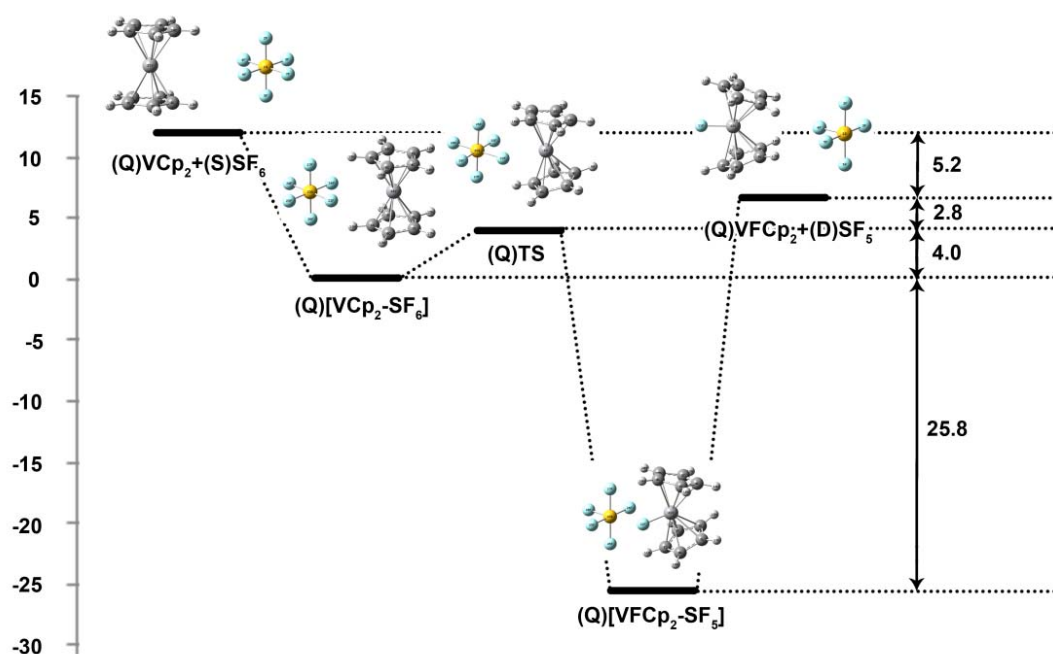


Fig. 4.15. Energy diagram for the monofluorination reaction of the high spin $^4\text{VCp}_2$. Energies are expressed in kcal mol^{-1} . In this picture, the inclusion of the transition state energy, shows a low barrier. The zero of the scale is arbitrarily set in reactants aggregate. The zero of the scale is arbitrarily set in reactants aggregate.

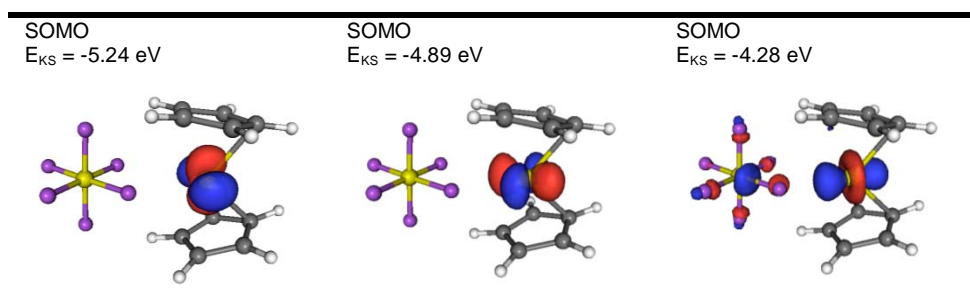


Fig. 4.16. Frontier orbitals of the transition state and their Kohn-Sham energies. The two lowest energy SOMO do not directly intervene in the transformation from reactives to products, but the other one, with its lobe pointing directly to the fluorine, shows an interaction with the $^1\text{SF}_6$.

The potential energy from the transition state to the supramolecule of products $^4(^3\text{VFCp}_2\text{-}^2\text{SF}_5)$ is of $29.8 \text{ kcal mol}^{-1}$, and the gain in potential energy of going from $^4(^3\text{VCp}_2\text{-}^1\text{SF}_6)$ to $^4(^3\text{VFCp}_2\text{-}^2\text{SF}_5)$ is of $25.8 \text{ kcal mol}^{-1}$, but this gain is lost when the two molecules that form the supramolecular product are separated.

4.3. A THERMODYNAMIC PROFILE FOR THE BI-FLUORINATION REACTION

The thermodynamic profile for bi-fluorination reaction (3.3) can be in an analogous way to the mono-fluorination. Fig. 4.17 shows geometries and total energies obtained for

${}^2[{}^2\text{VF}_2\text{Cp}_2\text{-}^1\text{SF}_4]$ and ${}^4[{}^4\text{VF}_2\text{Cp}_2\text{-}^1\text{SF}_4]$. The two structures are confirmed as minima with a frequencies calculation (Table 4.7).

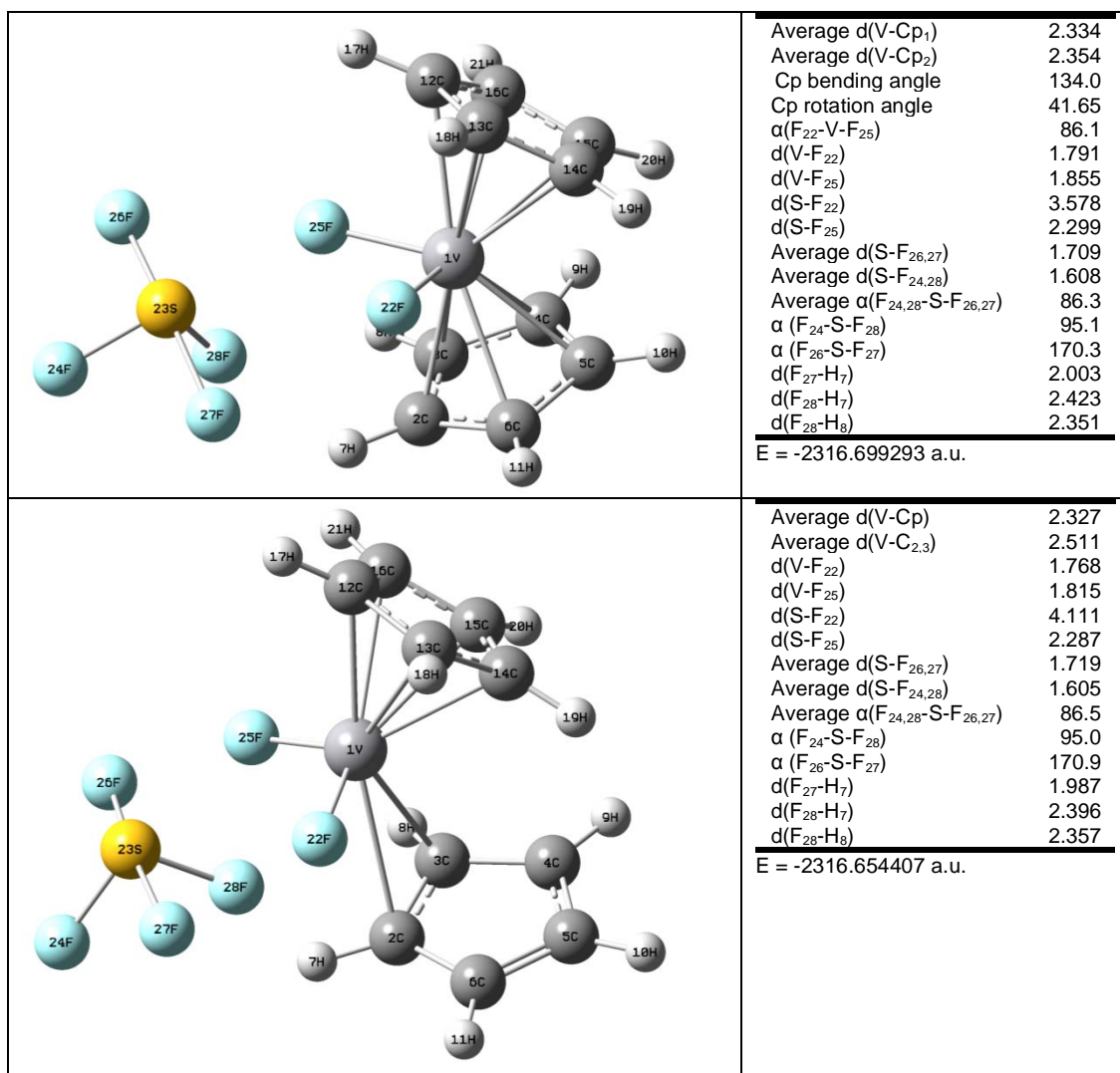


Fig. 4.17. Geometry of the ${}^2[{}^2\text{VF}_2\text{Cp}_2\text{-}^1\text{SF}_4]$ and ${}^4[{}^4\text{VF}_2\text{Cp}_2\text{-}^1\text{SF}_4]$ supramolecules. Distances are expressed in Angstroms, angles are expressed in degrees.

Table 4.7. The three lower frequency values for ${}^2[{}^2\text{VF}_2\text{Cp}_2\text{-}^1\text{SF}_4]$ and ${}^4[{}^4\text{VF}_2\text{Cp}_2\text{-}^1\text{SF}_4]$. All the values are in cm^{-1} . Experimental values are in parenthesis.

${}^2[{}^2\text{VF}_2\text{Cp}_2\text{-}^1\text{SF}_4]$	${}^4[{}^4\text{VF}_2\text{Cp}_2\text{-}^1\text{SF}_4]$
34.9	35.1
40.0	40.7
57.6	69.7

The energy diagram in Fig. 4.18 shows the relative energy differences between isolated reactants and products and the respective aggregates. The heat of formation for ${}^2[{}^2\text{VF}_2\text{Cp}_2\text{-}^1\text{SF}_4]$ and ${}^4[{}^4\text{VF}_2\text{Cp}_2\text{-}^1\text{SF}_4]$ is of $24.2 \text{ kcal mol}^{-1}$ and $24.3 \text{ kcal mol}^{-1}$ respectively. In an analogous way to the supramolecule ${}^4[{}^3\text{VFCp}_2\text{-}^2\text{SF}_5]$

(section 4.3.1) the stabilizing contribution to the energy of those aggregates comes from $\text{H}\cdots\text{F}$ interactions and dipole-dipole interactions. Fig. 4.19 shows the permanent dipole that exists in SF_4 and in VF_2Cp_2 and how in the supramolecule the two dipoles are

oriented to effectively interact. Due to time limitations, the transition states could not be computed, but will be obtained later on. Such transition state must exist or otherwise the VFCp₂ aggregate would not be stable.

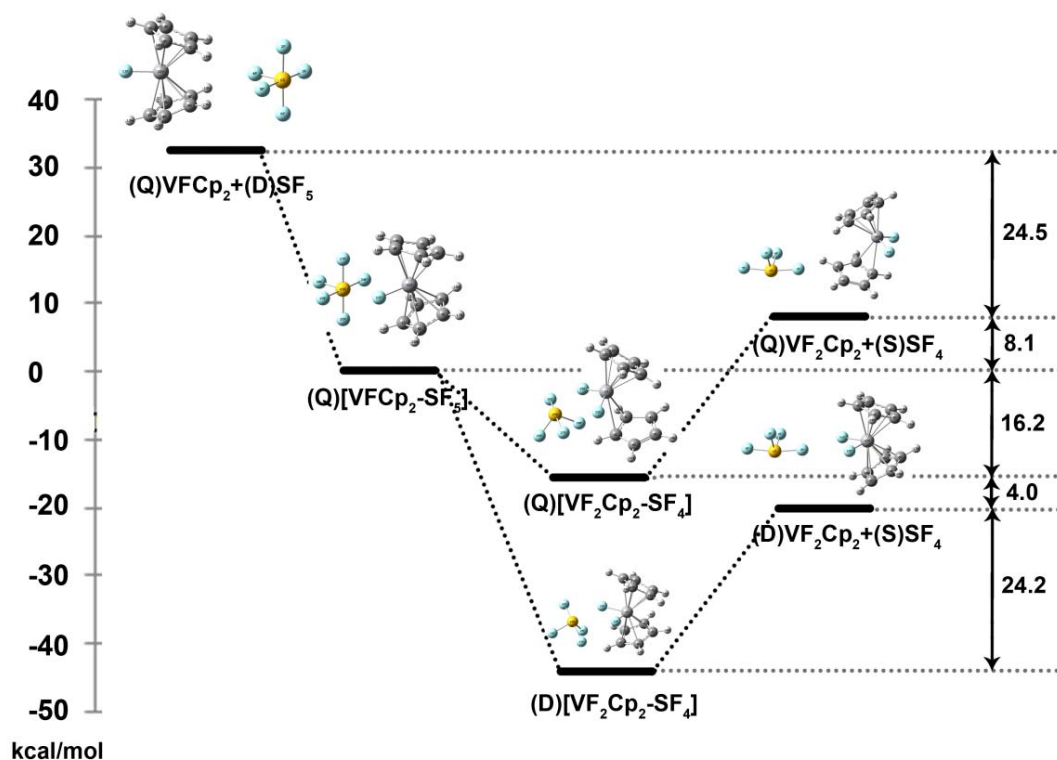


Fig. 4.18. Energy diagram for the fluorination reaction of ³VFCp₂ with ²SF₅. ³VFCp₂+²SF₅ are the reactives calculated separately; ⁴(VFCp₂-SF₅) represents the supramolecule of reactives. ⁴VF₂Cp₂+¹SF₄ and ²VF₂Cp₂+¹SF₄ are the high spin and low spin separate products; while ⁴(VF₂Cp₂+SF₄) and ²(VF₂Cp₂+SF₄) are the high spin and low spin products supramolecules. The zero of the E scale is arbitrarily placed in reactants aggregate.

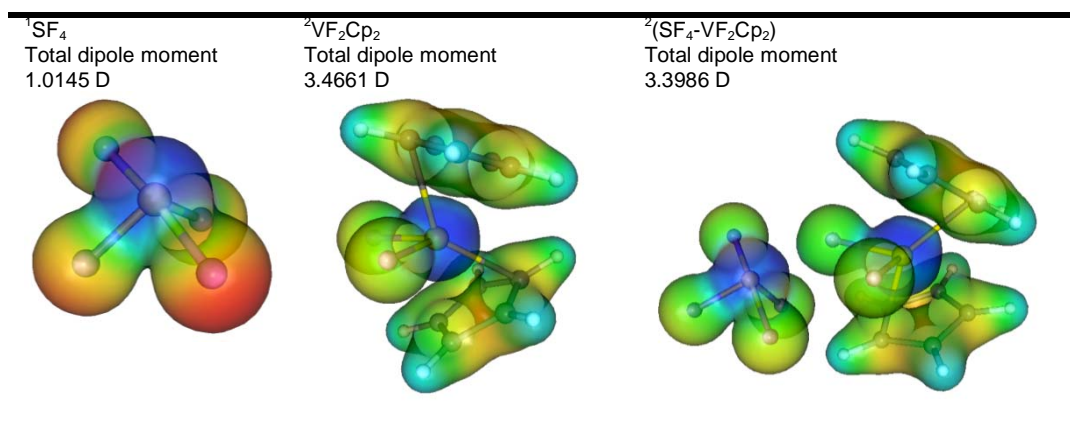


Fig. 4.19. Electron density and values of dipole moment for ¹SF₄, ⁴VF₂Cp₂ and ²(¹SF₄-⁴VF₂Cp₂).

A curve for the formation of the aggregates from the isolated molecules was not done for time reasons.

Although ${}^2\text{VCp}_2$ is $39.8 \text{ kcal mol}^{-1}$ higher than ${}^4\text{VCp}_2$, a thermodynamic study of reactions 4.2 and 4.3 (and 4.6) geometry optimizations of the corresponding supramolecules [i.e. ${}^2({}^2\text{VCp}_2\text{-}^1\text{SF}_6)$ for 4.2 and 4.3 and ${}^2({}^1\text{VFCp}_2\text{-}^2\text{SF}_5)$ for 4.6] was done. All of them yielded directly ${}^2({}^2\text{VF}_2\text{Cp}_2\text{-}^1\text{SF}_4)$ –Fig. 4.19 shows the resulting structure, with two fluorine atoms bound to vanadium but with a slightly different position of the SF_4 molecule respect to the VF_2Cp_2 geometry than in Fig. 4.16. The structure in Fig. 4.19 has an energy $1.9 \text{ kcal mol}^{-1}$ smaller than the ${}^2({}^2\text{VF}_2\text{Cp}_2\text{-}^1\text{SF}_4)$ structure in Fig. 4.16, and it has been confirmed to be a minimum with a frequencies calculation (the three lowest frequencies are of $11.0, 42.7$ and 54.6 cm^{-1}). Consequently in reaction 4.2 the transference of fluorine atoms to the low spin ${}^2\text{VCp}_2$ and ${}^1\text{VFCp}_2$ molecules takes place without kinetic barrier.

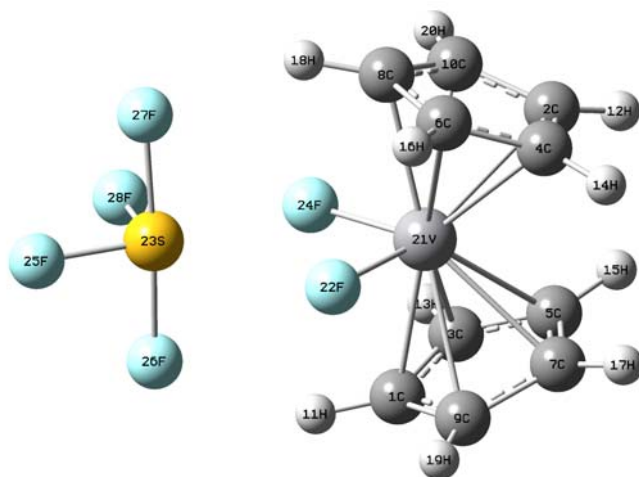


Fig. 4.20. ${}^2({}^2\text{VF}_2\text{Cp}_2\text{-}^1\text{SF}_4)$. Structure obtained from the optimization of ${}^2({}^2\text{VCp}_2\text{-}^1\text{SF}_6)$ and ${}^2({}^1\text{VFCp}_2\text{-}^2\text{SF}_5)$.

5. CONCLUSIONS

- The ground states for the vanadocene compounds are the high spin species in the case of the non-fluorinated and the mono-fluorinated species. However, the ground state of the bi-fluorinated vanadocene has a low spin doublet electronic configuration. ${}^4\text{VCp}_2$ shows a parallel disposition of the two Cp rings. In the case of the ${}^2\text{VCp}_2$, the two rings are bent. However, the fact that a theoretical minimum was not fully achieved for this system (not all frequencies are negative) does not allow us to confirm this statement.
- The ${}^4\text{VF}_2\text{Cp}_2$ structure shows a decrease in the hapticity of one of the two Cp rings, this could be explained by the occupation of a high spin orbital with anti-bonding vanadium – Cp π -orbital character that appears when a second fluorine atom combines with the frontier orbitals of the VFCp_2 .
- For the first fluorination ($\text{SF}_6 + \text{VCp}_2 \rightarrow \text{SF}_5 + \text{VFCp}_2$) the reaction has three stages:
 - 1) Reactants supramolecule formation from isolated reactants with a $\Delta E = -12.0 \text{ kcal mol}^{-1}$.
 - 2) Transference of one fluorine atom with a $\Delta E = -25.8 \text{ kcal mol}^{-1}$ and a transition state $4.0 \text{ kcal mol}^{-1}$ higher in energy than reactants.
 - 3) Isolated products formation from products supramolecule with a $\Delta E = 32.6 \text{ kcal mol}^{-1}$.Total $\Delta E = -5.2 \text{ kcal mol}^{-1}$.
- For the second fluorination ($\text{SF}_5 + \text{VFCp}_2 \rightarrow \text{SF}_4 + \text{VF}_2\text{Cp}_2$) the reaction has three stages:
 - 1) Reactants supramolecule formation from isolated reactants with a $\Delta E = -32.6 \text{ kcal mol}^{-1}$.
 - 2) Transference of one fluorine atom with a $\Delta E = -44.4 \text{ kcal mol}^{-1}$ (to yield ${}^2\text{VF}_2\text{Cp}_2$); $-16.2 \text{ kcal mol}^{-1}$ (to yield ${}^4\text{VF}_2\text{Cp}_2$).

3) Isolated products formation from products supramolecule with a $\Delta E = 24.2$ kcal mol⁻¹ (for ²VF₂Cp₂); 24.3 kcal mol⁻¹ (for ⁴VF₂Cp₂).

Total $\Delta E = -52.8$ kcal mol⁻¹ (²VF₂Cp₂); -24.5 kcal mol⁻¹ (⁴VF₂Cp₂).

- Fluorine transference to ²VCp₂ and ¹VFCp₂ (SF₆ + ²VCp₂ → SF₄ + ²VF₂Cp₂ and SF₅ + ¹VFCp₂ → SF₄ + ²VF₂Cp₂) takes place without a barrier and has two stages:

1) Products supramolecule formation from isolated reactants with a $\Delta E = -122.0$ kcal mol⁻¹ (from ²VCp₂); -86.6 kcal mol⁻¹.

2) Isolated products formation from products supramolecule with a $\Delta E = 24.2$ kcal mol⁻¹

Total $\Delta E = -97.8$ kcal mol⁻¹ (²VCp₂); -62.4 kcal mol⁻¹ (¹VFCp₂).

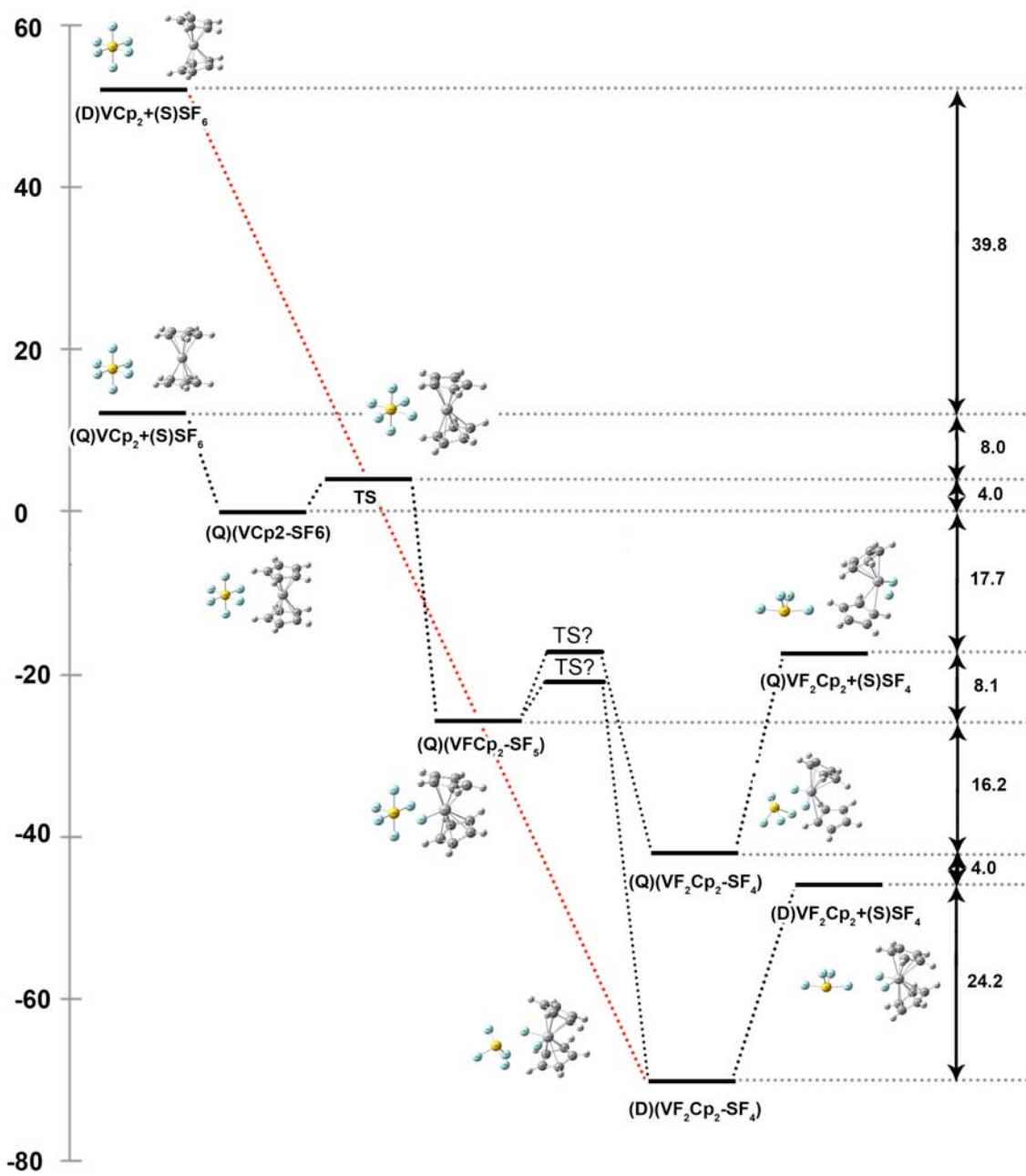


Fig. 5.1 Global energy diagram for the reactions studied.

6. BIBLIOGRAPHY

- [1] Harvey, B. G.; Arif, A. M.; Glöckner, A.; Ernst, R. D. *Organometallics* **2007**, *26*, 2872.
- [2] Paniagua, J. C.; Alemany, P. *Química Quántica I & II*, Llibres de l'Índex. Barcelona, Spain, 1999.
- [3] Szabo, A.; Ostlund, N. S. *Modern Quantum Chemistry Introduction to Advanced Electronic Structure Theory*, McGraw-Hill, Inc. 1989.
- [4] Born, M., Oppenheimer, J. R. *Ann. Physik.* **1928**, *84*, 457.
- [5] Andrés, J., Bertran, J. *Theoretical and Computational Chemistry: Foundations, methods and techniques*. Publicaciones de la Universitat Jaume I, Castelló de la Plana, Spain, 2007.
- [6] Baker, J. J. *Comput. Chem.* **1986**, *7*, 385.
- [7] Halgren, T. A.; Lipscomb, W. N. *Chem. Phys. Lett.* **1977**, *49*, 225.
- [8] Peng, C.; Ayala, P.Y.; Schlegel, H.B. *J. Comput. Chem.* **1996**, *17*, 49.
- [9] Levine, I. N. *Physical Chemistry*; McGraw-Hill, Inc., 1978.
- [10] Sinanoglu, A.; Brueckner, K.A. *Three Approaches to Electron Correlation in Atoms*. New Haven, Conn.: Yale University Press. 1970.
- [11] Hurley, A. C. *Electron Correlation in Small Molecules*. London: Academic Press. 1976.
- [12] Wilson, S. *Electron Correlation in Molecules*. Oxford: Clarendon Press. 1984.
- [13] Fermi, E. *Z. Phys.* **1928**, *48*, 73-79.
- [14] Thomas, L. H. *Proc. Camb. Phil. Soc.* **1927**, *23*, 542-548.
- [15] Hohenberg, P.; Kohn, W. *Phys. Rev. B* **1964**, *136*, 864-971.

- [16] Kohn, W.; Sham, L. J. *Phys. Rev. A* **1965**, *140*, 1133-1138.
- [17] Levy, M. *Phys. Rev. A* **1982**, *26*, 1200-1208.
- [18] Gaudoin, R.; Burke, K. *Phys. Rev. Lett.* **2004**, *93*, 173001-4.
- [19] Strowasser, A.; Hoffmann, R. *J. Am. Chem. Soc.* **1999**, *121*, 3414-3420.
- [20] Slater, J. C. *Quantum Theory of Molecules and Solids, Volume 4, The Self-Consistent Field for Molecules and Solids*. McGraw-Hill, New York, 1974.
- [21] Schwartz, K. *Phys. Rev. B* **1972**, *5*, 2466-2468.
- [22] von Barth, U.; Hedin, L. *J. Phys. C* **1972**, *5*, 1629-1642.
- [23] Gunnarsson, O.; Lundqvist, B. I. *Phys. Rev. B* **1976**, *13*, 4274-4298.
- [24] Vosko, S. J.; Wilk, L.; Nusair, M. *Can. J. Phys.* **1980**, *58*, 1200-1211.
- [25] Sousa, S. F.; Fernandes, P. A.; Ramos, M. J.; *J. Phys. Chem. A* **2007**, *111*, 10439-10452.
- [26] Becke, A. D. *Phys. Rev. A* **1988**, *38*, 3098-3100.
- [27] Perdew, J. P. *Phys. Rev. B* **1986**, *33*, 8822-8824.
- [28] Lee, C.; Yang, W.; Parr, R. G. *Phys. Rev. B* **1988**, *37*, 785-789.
- [29] Perdew, J. P.; Kurth, S.; Zupan, A.; Blaha, P. *Physical Review Letters* **1999**, *82* (12) 2544-2547.
- [30] Becke, A. D. *J. Chem. Phys.* **1996**, *104*, 1040.
- [31] Krieger, J. B.; Chen, J.; Iafrate, G.J.; Savin, A. *Electron. Correl. Mater. Prop.* **1999**, *463*.
- [32] Tao, J.; Perdew, J. P.; Staroverov, V. N.; Scuseria, G. E. *Phys. Rev. Lett.* **2003**, *91*, Art. No. 146401.
- [33] Van Voorhis, T.; Scuseria, G. E. *J. Chem. Phys.* **1998**, *109*, 400.

- [34] Perdew, J. P. *Unified Theory of Exchange and Correlation Beyond the Local Density Approximation*. In *Electronic Structure of Solids '91*; Ziesche, P.; Eschig, H.; Eds. Akademie Verlag: Berlin, Germany, 1991, pp 11-20.
- [35] Fischer, E. O.; Fritz, H. P. *Adv. Inorg. Chem. Radiochem.* **1959**, *1*, 55. Wilkinson, G.; Rosenblum, M.; Whiting, M. C.; Woodward, R. B. *J. Am. Chem. Soc.* **1952**, *74*, 2125, Woodward, R. B.; Rosenblum, M.; Whiting, M. C. *J. Am. Chem. Soc.* **1952**, *74*, 3458, Dunitz, J. D.; Orgel, E. *Nature (London)* **1953**, *171*, 121.
- [36] Andersen, A.; Cordes, H.-G.; Herwig, J.; Kaminsky, W.; Merck, A.; Mottweiler, R.; Pein, J.; Sinn, H.; Vollmer, H.-J. *Angew. Chem. Int. Ed. Engl.*, **1976**, *15*, 630.
- [37] Halterman, R. L.; *Chem. Rev.* **1992**, *92*, 969, Okuda, J. *Angew. Chem.* **1992**, *104*, 49, *Angew. Chem., Int. Ed. Engl.* **1992**, *31*, 47.
- [38] Shapiro, P. J. *Coord. Chem. Rev.*, **2002**, *231*, 67.
- [39] McGarrity, J.; Spindler, F.; Fuchs, R.; Eyer, M. Eur. Pat. Appl. EP 624 587 A2, (LONZA AG), *Chem. Abstr.* **1995**, *122*, P81369q.
- [40] Borman, S. *Chem. & Eng. News* **1996**, July 12, pp. 38-40.
- [41] Köpf-Maier, P.; Köpf, H. *Chem. Rev.* **1987**, *87*, 1137
- [42] Köpf, H.; Köpf-Maier, P. *Angew. Chem.* **1979**, *91*, 509, *Angew. Chem., Int. Ed. Engl.* **1979**, *18*, 477.
- [43] Honzicek, J.; Vinklerek, J.; Cernosek, Z.; Cisarova, I. *Magn. Reson. Chem.* **2007**, *45*, 508.
- [44] Choukroun, R.; Lorber, C.; de Caro, D.; Vendier, L. *Organometallics*, **2006**, *25*, 4243.
- [45] Arimoto, F. S.; Haven, A. C. *J. Am. Chem. Soc.* **1955**, *77*, 6295.
- [46] Togni, A.; Halterman, R. L. *Metallocenes: Synthesis, Reactivity, Applications*, Vol. 1 & 2 WILEY-VCH- VERLAG GMBH, D-69469 Weinheim (Federal Republic of Germany), 1998.
- [47] Doyle, G.; Tobias, R. S. *Inorg. Chem.* **1968**, *7*, 12, 2479.

- [48] Ghosh, P.; D'Cruz, O. J.; DuMez, D. D.; Uckun, F. M. *J. Inorg. Biochem.* **1999**, *74*, 322.
- [49] Karapinka, G. L.; Carrick, W. L. *J. Polym. Sci.* **1961**, *55*, 145.
- [50] Breslow, D. S. *Chem. Abstr.* **1960**, *54*, 11573.
- [51] Sinn, H.; Kaminsky, W.; Vollmer, H. J.; Woldt, R. *Angew. Chem., Int. Ed. Engl.* **1980**, *19*, 390.
- [52] Zhen-Feng Xu; Yaoming Xie; Wen-Lin Feng; Schaefer, H. F., III *J. Phys. Chem. A* **2003**, *107*, 2716.
- [53] Hargittai, R. J.; Gillespie, I. *The VSEPR Model of Molecular Geometry*; Allyn and Bacon: Needham Heights, 1991.
- [54] Albright, T. A.; Burdett, J. K.; Whangbo, M.-H. *Orbital Interactions In Chemistry*, John Wiley & Sons, Inc. 1985
- [55] Green, J. C. *Chem. Soc. Rev.* **1998**, *27*, 263
- [56] Lyssenko, K. A.; Golovanov, D. G.; Antipin, M. Y. *Mendeleev Commun.* **2003**, *13*, 5, 209.
- [57] Tsai, W.-T. *Journal of Fluorine Chemistry* **2007**, *128*, 1345.
- [58] <http://unfccc.int/resource/docs/convkp/kpeng.html>
- [59] American Conference of Governmental Industrial Hygienists (ACGIH), Documentation of the Threshold Limit Values and Biological Exposure Indices, ACGIH, Cincinnati, Ohio, USA, 2002.
- [60] Occupational Safety and Health Administration (OSHA), Safety and Health Topics: Permissible Exposure Limits (PELs), 2003, available: <http://www.osha.gov/SLTC/pel/index.html> (accessed 8 February 2007).
- [61] Council of Labor (COLA), Permissible Concentration Standards of Air Toxics at Workplace Environment (in Chinese), COLA, Taipei, Taiwan, 2003.
- [62] Harvey, B. G.; Arif, A. M.; Glöckner, A.; Ernst, R. D. *Organometallics* **2007**, *26*, 2872.

- [63] Basta, R.; Harvey, B. G.; Arif, A. M.; Ernst, R. D. *J. Am. Chem. Soc.* **2005**, *127*, 11924.
- [64] Cheung, Y.-S.; Chen, Y.-J.; Ng, C. Y.; See-Wing Chiu; Wai-Kee Li *J. Am. Chem. Soc.* **1995**, *117*, 9725.
- [65] Pauling, L. *J. Am. Chem. Soc.* **1931**, *53*, 1367.
- [66] Lewis, G. N. *J. Am. Chem. Soc.* **1916**, *38*, 762.
- [67] Langmuir, J. *J. Am. Chem. Soc.* **1919**, *41*, 868.
- [68] Rundle, R. E. *J. Am. Chem. Soc.* **1947**, *69*, 1327. *J. Am. Chem. Soc.* **1963**, *85*, 112.
- [69] Pimentel, G. C. *J. Chem. Phys.* **1951**, *19*, 446.
- [70] Woon, E. D.; Dunning, T. H. *J. Phys. Chem.* **2009**, *113*, 7915.
- [71] Reed, A. E.; Weinbold, F. *J. Am. Chem. Soc.*, **1986**, *108*, 3586.
- [72] Irikura, K. K. *J. Chem. Phys.* **1995**, *102*, 5357.
- [73] Ziegler, T.; Gutsev, G. L. *J. Chem. Phys.* **1992**, *96*, 7623.
- [74] Tolles, W. M.; Gwinn, W. D. *J. Chem. Phys.* **1962**, *36*, 1119.
- [75] Ischenko, A. A.; Ewbank, J. D.; Schäfer, L. *J. Phys. Chem.* **1994**, *98*, 4287.
- [76] J. S. Binkley, J. A. Pople, and W. J. Hehre *J. Am. Chem. Soc.*, **102** (1980) 939-47.
- [77] M. S. Gordon, J. S. Binkley, J. A. Pople, W. J. Pietro, and W. J. Hehre *J. Am. Chem. Soc.*, **104** (1982) 2797-803.
- [78] W. J. Pietro, M. M. Francl, W. J. Hehre, D. J. Defrees, J. A. Pople, and J. S. Binkley *J. Am. Chem. Soc.*, **104** (1982) 5039-48.
- [79] K. D. Dobbs and W. J. Hehre *J. Comp. Chem.*, **7** (1986) 359-78.
- [80] K. D. Dobbs and W. J. Hehre *J. Comp. Chem.*, **8** (1987) 861-79.
- [81] K. D. Dobbs and W. J. Hehre *J. Comp. Chem.*, **8** (1987) 880-93.
- [82] Gaussian 03, Revision D.02, M. J. Frisch, G. W. Trucks, H. B. Schlegel, G. E.

Scuseria, M. A. Robb, J. R. Cheeseman, J. A. Montgomery, Jr., T. Vreven, K. N. Kudin, J. C. Burant, J. M. Millam, S. S. Iyengar, J. Tomasi, V. Barone, B. Mennucci, M. Cossi, G. Scalmani, N. Rega, G. A. Petersson, H. Nakatsuji, M. Hada, M. Ehara, K. Toyota, R. Fukuda, J. Hasegawa, M. Ishida, T. Nakajima, Y. Honda, O. Kitao, H. Nakai, M. Klene, X. Li, J. E. Knox, H. P. Hratchian, J. B. Cross, V. Bakken, C. Adamo, J. Jaramillo, R. Gomperts, R. E. Stratmann, O. Yazyev, A. J. Austin, R. Cammi, C. Pomelli, J. W. Ochterski, P. Y. Ayala, K. Morokuma, G. A. Voth, P. Salvador, J. J. Dannenberg, V. G. Zakrzewski, S. Dapprich, A. D. Daniels, M. C. Strain, O. Farkas, D. K. Malick, A. D. Rabuck, K. Raghavachari, J. B. Foresman, J. V. Ortiz, Q. Cui, A. G. Baboul, S. Clifford, J. Cioslowski, B. B. Stefanov, G. Liu, A. Liashenko, P. Piskorz, I. Komaromi, R. L. Martin, D. J. Fox, T. Keith, M. A. Al-Laham, C. Y. Peng, A. Nanayakkara, M. Challacombe, P. M. W. Gill, B. Johnson, W. Chen, M. W. Wong, C. Gonzalez, and J. A. Pople, Gaussian, Inc., Wallingford CT, 2004.

[83] Ischenko, A. A.; Ewbank, J. D.; Schäfer, L. *J. Phys. Chem.* **1994**, *98*, 4287.

[84] Tolles, W. M.; Gwinn, W. D. *J. Chem. Phys.* **1962**, *36*, 1119.

[85] Miller, T. M.; Arnold, S. T.; Viggiano, A. A. *Int. J. Mass. Spectrom.* **2003**, *227*, 413.

[86] Kiang, T.; Zare, R. N. *J. Am. Chem. Soc.* **1980**, *102*, 4024.

[87] Lias, S. G.; Bartmess, J. E.; Liebman, J. F.; Holmes, J. L.; Levin, R. D.; Mallard, W. G. *J. Phys. Chem. Ref. Data* **1988**, *17*, Suppl. No. 1.

[88] D'Oria, E.; Novoa, J. J. *CrystEngComm* **2008**, *10*, 423.

[89] Shimanouchi, T. *Tables of Molecular Vibrational Frequencies, Consolidated Volume I* (U.S. GPO, Washington, D.C., 1972).

[90] Christe, K. O.; Sawodny, W. *J. Chem. Phys.* **1970**, *52*, 6320.

[91] Levin, I. W.; Berney, C. V. *J. Chem. Phys.* **1966**, *44*, 2557.

7. APPENDICES

A1. Specific keywords utilized on Gaussian03 calculations:

Nosymm: Disables the use of the *standard orientation* coordinates and the use of molecular symmetry within the calculation.

OPT:

VERYTIGHT: Extremely tight optimization convergence criteria.

TS: Looks for a 1st order saddle point.

NOEIGENTEST: Suppresses testing the curvature in Berny optimizations. Diminishes the calculation costs.

CALCF: Specifies that the force constants be computed at the first point using the current method.

INTEGRAL:

ULTRAFINE: Recommended to use along the verytight keyword for DFT calculations and for computing very low frequency modes of systems.

SCF:

XQC: Involves linear searches when far from convergence and Newton-Raphson steps when close. In case the first order SCF has not converged, adds an extra QC.

NOVARACC: Disables the use modest integral accuracy early in direct SCF.

GUESS:

ALWAYS: Requests that a new initial guess be generated at each point of an optimization.

A2. Mulliken atomic charges and Mulliken atomic spin densities of the isolated reactives ${}^1\text{SF}_6$, ${}^4\text{VCp}_2$ and products ${}^2\text{SF}_5$, ${}^3\text{VFCp}_2$, and of the supramolecules ${}^4({}^4\text{VCp}_2-{}^1\text{SF}_6)$, ${}^4({}^3\text{VFCp}_2-{}^2\text{SF}_5)$.

A2.1.

Mulliken atomic charges -Reactives				
		${}^4({}^4\text{VCp}_2-{}^1\text{SF}_6)$	${}^1\text{SF}_6, {}^4\text{VCp}_2$	Differenc e
C	1	-0,34741	-0,342229	-0,005181
C	2	-0,342003	-0,342114	0,000111
C	3	-0,346874	-0,342275	-0,004599
C	4	-0,340578	-0,342276	0,001698
C	5	-0,340926	-0,342567	0,001641
C	6	-0,347981	-0,342526	-0,005455
C	7	-0,341564	-0,342096	0,000532
C	8	-0,346533	-0,342197	-0,004336
C	9	-0,345501	-0,342427	-0,003074
C	10	-0,344679	-0,342315	-0,002364
H	11	0,175538	0,204214	-0,028676
H	12	0,203507	0,204219	-0,000712
H	13	0,203443	0,204219	-0,000776
H	14	0,203307	0,204209	-0,000902
H	15	0,203346	0,204194	-0,000848
H	16	0,203161	0,204212	-0,001051
H	17	0,203464	0,204223	-0,000759
H	18	0,174421	0,204197	-0,029776
H	19	0,203839	0,204215	-0,000376
H	20	0,203778	0,204205	-0,000427
V	21	1,32296	1,380916	-0,057956
F	22	-0,262425	-0,281595	0,01917
S	23	1,740014	1,689567	0,050447
F	24	-0,263448	-0,281595	0,018147
F	25	-0,268874	-0,281595	0,012721
F	26	-0,266354	-0,281595	0,015241
F	27	-0,266963	-0,281595	0,014632
F	28	-0,268667	-0,281595	0,012928

A2.2.

Mulliken atomic spin densities -Reactives				
		${}^4({}^4\text{VCp}_2-{}^1\text{SF}_6)$	${}^1\text{SF}_6, {}^4\text{VCp}_2$	Difference
C	1	0,01565	0,011877	0,003773
C	2	0,009241	0,011818	-0,002577
C	3	0,011295	0,011883	-0,000588
C	4	0,010289	0,011845	-0,001556
C	5	0,010266	0,011857	-0,001591
C	6	0,011181	0,011856	-0,000675
C	7	0,00937	0,011868	-0,002498
C	8	0,015616	0,011881	0,003735
C	9	0,010647	0,01183	-0,001183
C	10	0,010759	0,011835	-0,001076
H	11	0,002838	0,00305	-0,000212
H	12	0,003004	0,003047	-4,3E-05
H	13	0,003266	0,003052	0,000214
H	14	0,002961	0,003057	-9,6E-05
H	15	0,002986	0,003068	-0,000082
H	16	0,003279	0,003061	0,000218
H	17	0,002982	0,003049	-6,7E-05
H	18	0,002858	0,00306	-0,000202
H	19	0,003197	0,003059	0,000138
H	20	0,003175	0,003058	0,000117
V	21	2,852594	2,850888	0,001706
F	22	0,00048	-	0,00048
S	23	0,00083	-	0,00083
F	24	0,000443	-	0,000443
F	25	0,00016	-	0,00016
F	26	0,000246	-	0,000246
F	27	0,000258	-	0,000258
F	28	0,000134	-	0,000134

A2.3.

Mulliken atomic charges -Products				
		$^4(^3\text{VFCp}_2\text{-}^2\text{SF}_5)$	$^2\text{SF}_5, ^3\text{VFCp}_2$	Difference
C	1	-0,310505	-0,215185	0,09532
C	2	-0,345804	-0,329513	0,016291
C	3	-0,318182	-0,343816	-0,025634
C	4	-0,325284	-0,330576	-0,005292
C	5	-0,330087	-0,330253	-0,000166
C	6	-0,340161	-0,343654	-0,003493
C	7	-0,314387	-0,330272	-0,015885
C	8	-0,262677	-0,215872	0,046805
C	9	-0,322048	-0,343711	-0,021663
C	10	-0,318801	-0,343577	-0,024776
H	11	0,228939	0,228063	-0,000876
H	12	0,217797	0,20845	-0,009347
H	13	0,228202	0,215916	-0,012286
H	14	0,215511	0,208884	-0,006627
H	15	0,213178	0,208608	-0,00457
H	16	0,221372	0,216133	-0,005239
H	17	0,218902	0,208675	-0,010227
H	18	0,23353	0,228044	-0,005486
H	19	0,228377	0,215995	-0,012382
H	20	0,228834	0,215862	-0,012972
V	21	1,279538	1,310735	0,031197
F	22	-0,321868	-0,338936	-0,017068
S	23	1,458812	1,442404	-0,016408
F	24	-0,297266	-0,293092	0,004174
F	25	-0,287222	-0,293092	-0,00587
F	26	-0,296143	-0,292844	0,003299
F	27	-0,306223	-0,292945	0,013278
F	28	-0,276332	-0,270431	0,005901

A2.4.

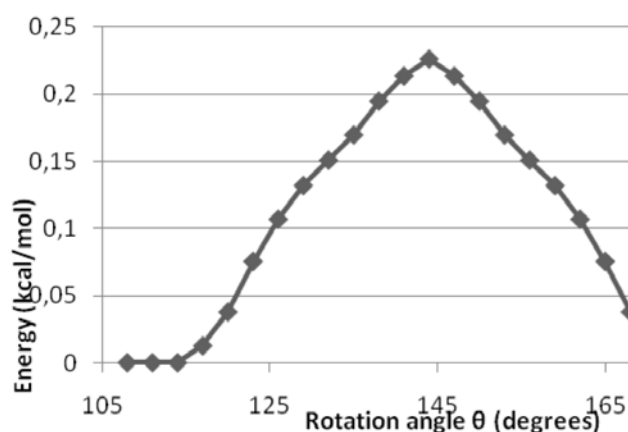
Mulliken atomic spin densities -Products				
		$^4(^3\text{VFCp}_2\text{-}^2\text{SF}_5)$	$^2\text{SF}_5, ^3\text{VFCp}_2$	Difference
C	1	-0,007542	-0,056069	0,048527
C	2	-0,040128	-0,026471	-0,013657
C	3	-0,009282	0,042784	-0,052066
C	4	-0,033452	-0,030503	-0,002949
C	5	-0,010583	-0,028348	0,017765
C	6	0,03744	0,044425	-0,006985
C	7	-0,039011	-0,028861	-0,01015
C	8	-0,066816	-0,055806	-0,01101
C	9	0,009446	0,043241	-0,033795
C	10	0,04895	0,041155	0,007795
H	11	0,000226	0,002692	-0,002466
H	12	0,003642	0,002953	0,000689
H	13	0,002359	0,000299	0,00206
H	14	0,002941	0,003336	-0,000395
H	15	0,000778	0,003139	-0,002361
H	16	0,000791	0,000208	0,000583
H	17	0,003785	0,003182	0,000603
H	18	0,002859	0,002682	0,000177
H	19	0,001026	0,000266	0,00076
H	20	-0,000647	0,000374	-0,001021
V	21	2,09203	2,004271	0,087759
F	22	0,12748	0,031049	0,096431
S	23	0,351803	0,441019	-0,089216
F	24	0,141205	0,141412	-0,000207
F	25	0,121788	0,141412	-0,019624
F	26	0,131371	0,141173	-0,009802
F	27	0,12902	0,140967	-0,011947
F	28	-0,00148	-0,005982	0,004502

A2.5.

Transition State		Mulliken atomic charges	Mulliken atomic spin density
1	V	1,237393	2,730975
2	C	-0,318674	0,018977
3	C	-0,339663	-0,003687
4	C	-0,342095	-0,006404
5	C	-0,329327	0,005116
6	C	-0,336332	0,003354
7	H	0,197174	0,000572
8	H	0,21048	0,003094
9	H	0,208002	0,002534
10	H	0,208302	0,00255
11	H	0,208317	0,002417
12	C	-0,342356	0,018303
13	C	-0,307794	0,005588
14	C	-0,340333	0,006929
15	C	-0,338158	-0,008879
16	C	-0,341673	-0,002746
17	H	0,20245	0,001415
18	H	0,20408	0,00134
19	H	0,207342	0,002673
20	H	0,208248	0,002886

21	H	0,209553	0,002834
22	F	-0,264173	0,005495
23	S	1,699194	0,092578
24	F	-0,279001	0,030034
25	F	-0,280483	0,021493
26	F	-0,284184	0,025019
27	F	-0,280693	0,027561
28	F	-0,275595	0,007979

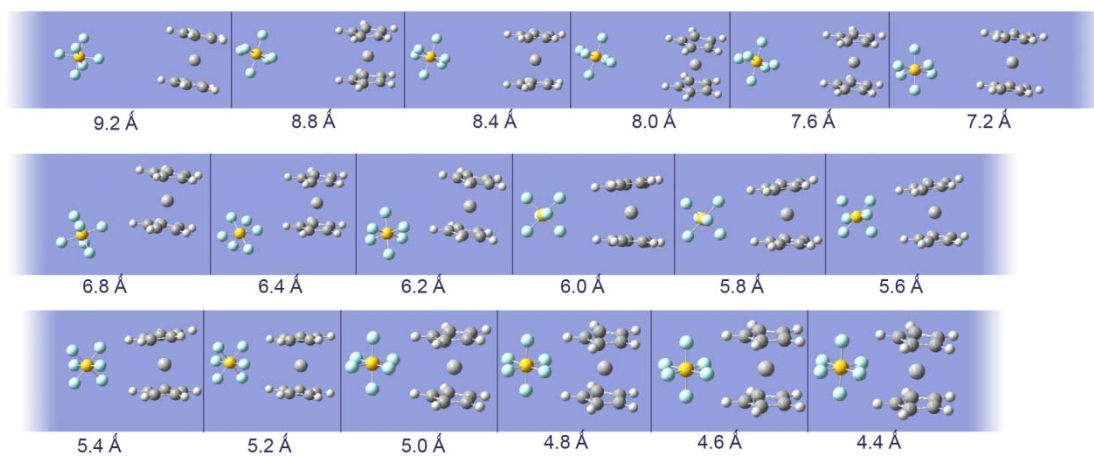
A3. Rotational barrier of the cyclopentadienyl rings of ${}^4\text{VCp}_2$ at the B3LYP/3-21G* level. Relative energy is expressed in kcal mol $^{-1}$.



Angle θ	Relative energy	Angle θ	Relative energy
180	0,00	141	0,21
177	0,00	138	0,19
174	0,00	135	0,17
171	0,01	132	0,15
168	0,04	129	0,13
165	0,08	126	0,11
162	0,11	123	0,08
159	0,13	120	0,04
156	0,15	117	0,01
153	0,17	114	0,00
150	0,19	111	0,00
147	0,21	108	0,00
144	0,23		

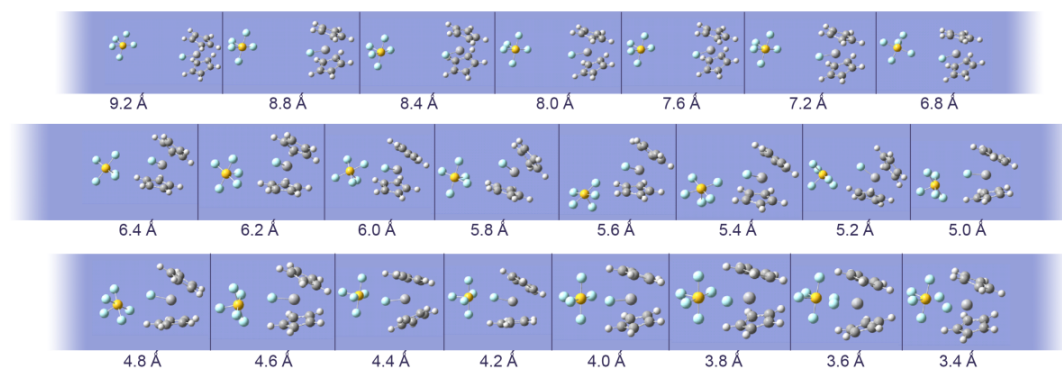
A4. Scheme showing the optimized geometries at different S-V distances, for the separation of the supramolecules of reactives and products; as well as the corresponding energy values for each distance. The distances under each picture are S-V distance values. Distances of the tables are in Å, and relative energies are in kcal mol $^{-1}$.

A4.1. Reactives



d(S-V)	Relative energy	d(S-V)	Relative energy
4,4	-0,1	6,2	6,5
4,6	0,0	6,4	7,4
4,8	0,8	6,8	8,2
5	2,0	7,2	10,8
5,2	2,5	7,6	11,2
5,4	3,3	8	11,3
5,6	4,3	8,4	11,7
5,8	5,1	8,8	11,8
6	6,4	9,2	11,6

A4.2. Products



A5. Energy values for potential energy curves using the S-F distance as the reaction coordinate. Distances are in Å and energies in kcal mol⁻¹.

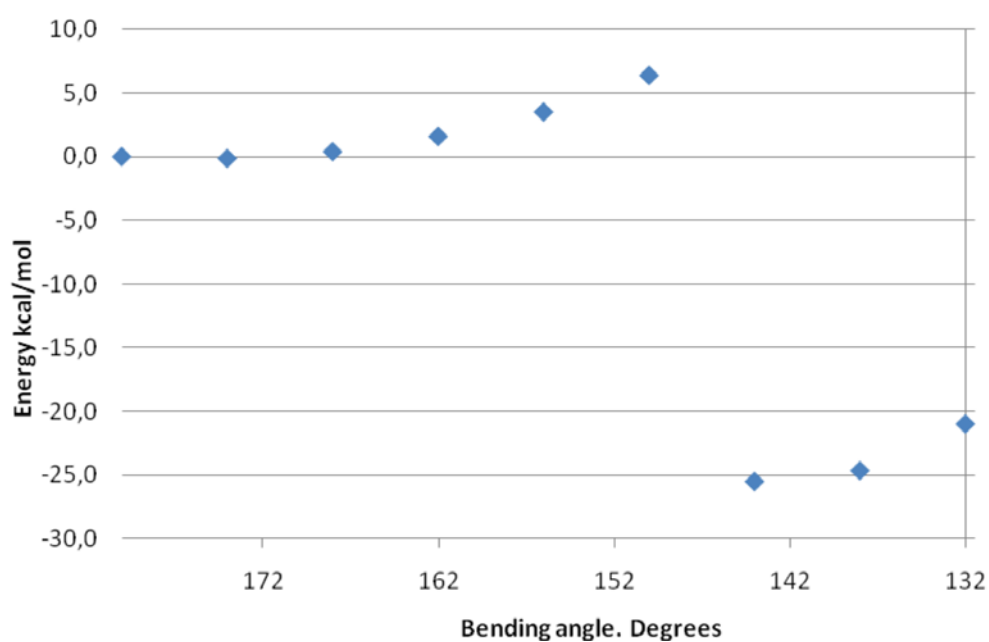
Potential energy curve built from reactives to products.

d(S-F)	Relative energy	d(S-F)	Relative energy
1,592	0,0	1,790	-14,3
1,650	1,0	1,800	-14,7
1,700	3,5	1,900	-18,9
1,750	6,8	2,000	-22,5
1,760	7,6	2,100	-24,7
1,770	8,3	2,200	-25,6
1,780	9,1	2,245	-25,7

Potential energy curve built from products to reactives. Shadowed values correspond to geometries in which the distance between the sulfur atom and the second fluorine atom closer to the vanadium was fixed to be 1.631 Å.

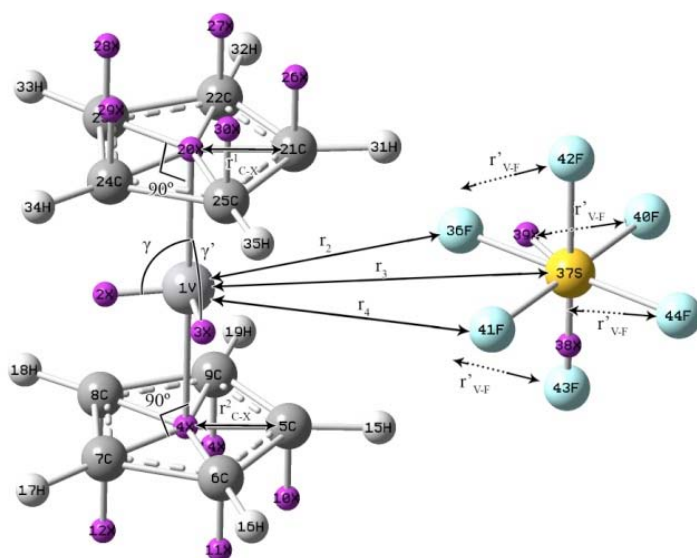
d(S-F)	Relative energy	d(S-F)	Relative energy
1,650	-25,1	2,100	-24,7
1,700	-25,6	2,200	-25,6
1,710	-25,7	2,245	-25,7
1,720	-25,7	1,550	1,5
1,730	-25,6	1,575	0,8
1,740	-25,6	1,600	0,8
1,750	-12,6	1,650	4,6
1,790	-14,3	1,675	1,9
1,800	-14,7	1,700	-0,6
1,900	-18,9	1,725	-3,0
2,000	-22,5		

A6. Potential energy curve representing the bending angle γ versus the relative energy, and the respective tabulated numerical values of the curve. Angle values are in degrees, and energies in kcal mol⁻¹.



Bending angle γ	Relative energy
180	0,0
174	-0,1
168	0,4
162	1,6
156	3,5
150	6,4
144	-25,5
138	-24,7
132	-21,0

A.7. Illustration of the z-matrix used to build the potential energy surface, an explanation of its structural constraints and an example of z-matrix directly taken from an input.



- r^1_{C-X} and r^2_{C-X} represent the distances between each of the carbon atoms of one ring and its centroid (where a dummy is located). All the C-X distances belonging to the same ring are imposed to be equal, to force the dummy to be in the center of the ring. A consequence is that cyclopentadienyls are forced to be regular pentagons.

- The angle formed by each carbon atom, the dummy atom in the center of the ring and the vanadium atom is imposed to be of 90° . This restriction allows to properly control the relative inclination of the two Cp rings.

- γ and γ' are the two orthogonal angles that determine the overall relative inclination of the Cp rings. Their values are independent, and the variation of one of those angles does not affect the value of the other one, for that reason one of them is imposed to be of 90° , thus remaining the non-constrained angle as the unique coordinate that determines the bending of the Cp rings. Note that the bending angle (as it is defined in Fig. 3.5) corresponds to two times the value of angle γ as it is depicted on the present z-matrix. In the z-matrix, the upper and lower angle are defined by the same variable, which means that the vanadocene described by this matrix bends in a symmetrical fashion.

- r_2 represents the distance between the fluorine atom that is to be transferred and the vanadium. r_4 is the distance between the second fluorine atom closest to the vanadium and the vanadium atom itself. r_3 is the distance between the sulfur atom and the vanadium atom. All three distances are well defined as explicit variables in the z-matrix. Specifically, r_2 and r_4 must be defined with respect to the vanadium atom since both of them need to be fixed in some or all the points of the surface.

- r'_{V-F} represent the distances between each of the remaining fluorine atoms and the vanadium atom. In most of the points of the surface, the fluorine atoms are defined in relation to the sulfur atom and the two dummies attached to it. However, in a few points (see Fig. 4.15) all the distances V-F are fixed to avoid an unwanted approach of a fluorine atom to the vanadium. In that particular case, the two dummies attached to the sulfur atom are useless.

Z-matrix used to calculate the (3.5 Å, 180°) point of the potential energy surface.

1	V					
2	X	1	1,0			
3	X	1	1,0	2	90,0	
4	X	1	B1	2	A1	3 90,0
5	C	4	B2	1	90,0	2 D2
6	C	4	B2	1	90,0	5 D3
7	C	4	B2	1	90,0	5 D4
8	C	4	B2	1	90,0	5 D5
9	C	4	B2	1	90,0	5 D6
10	X	5	1,0	4	90,0	1 180,0
11	X	6	1,0	4	90,0	1 180,0
12	X	7	1,0	4	90,0	1 180,0
13	X	8	1,0	4	90,0	1 180,0
14	X	9	1,0	4	90,0	1 180,0
15	H	5	B7	10	A7	4 D7
16	H	6	B8	11	A8	4 D8
17	H	7	B9	12	A9	4 D9
18	H	8	B10	13	A10	4 D10
19	H	9	B11	14	A11	4 D11
20	X	1	B12	2	A1	3 -90,0
21	C	20	B13	1	90,0	2 D13
22	C	20	B13	1	90,0	21 D14
23	C	20	B13	1	90,0	21 D15
24	C	20	B13	1	90,0	21 D16
25	C	20	B13	1	90,0	21 D17
26	X	21	1,0	20	90,0	1 180,0
27	X	22	1,0	20	90,0	1 180,0
28	X	23	1,0	20	90,0	1 180,0
29	X	24	1,0	20	90,0	1 180,0
30	X	25	1,0	20	90,0	1 180,0
31	H	21	B18	26	A18	20 D18
32	H	22	B19	27	A19	20 D19
33	H	23	B20	28	A20	20 D20
34	H	24	B21	29	A21	20 D21
35	H	25	B22	30	A22	20 D22
36	F	1	B23	4	A23	3 D23
37	S	1	B24	4	A24	3 D24
38	X	37	1,0	1	90,0	4 D25
39	X	37	1,0	38	90,0	1 D26
40	F	37	B25	38	A25	39 D27
41	F	1	B26	4	A26	3 D28
42	F	37	B27	39	A27	38 D29
43	F	37	B28	39	A28	38 D30
44	F	37	B29	38	A29	39 D31
<hr/>						
	B1	2,00				
	B2	1,25				

B2 are the C- X_{centroid} distances, all of them equivalent. The C- X_{centroid} -V angle is fixed to 90°.

B13 are the C- X_{centroid} distances of the second Cp ring and are also equivalent. The C- X_{centroid} -V angle for this second ring is also fixed to 90°.

The distance V-F is defined by B23

The distance V-F is defined by B26

B7	1,10	
B8	1,10	
B9	1,10	
B10	1,10	
B11	1,10	
B12	2,00	
B13	1,25	
B18	1,10	
B19	1,10	
B20	1,10	
B21	1,10	
B22	1,10	
B24	4,43	
B25	1,60	
B27	1,60	
B28	1,60	
B29	1,60	
A7	90,0	
A8	90,0	
A9	90,0	
A10	90,0	
A11	90,0	
A18	90,0	
A19	90,0	
A20	90,0	
A21	90,0	
A22	90,0	
A23	90,0	
A24	90,0	
A25	90,0	
A26	90,0	
A27	90,0	
A28	90,0	
A29	90,0	
D2	180,0	
D3	72,0	
D4	144,0	
D5	-144,0	
D6	-72,0	
D7	180,0	
D8	180,0	
D9	-180,0	
D10	180,0	
D11	180,0	
D13	180,0	
D14	72,0	
D15	144,0	
D16	-144,0	
D17	-72,0	
D18	180,0	
D19	180,0	
D20	180,0	
D21	180,0	
D22	180,0	
D23	90,0	
D24	72,0	
D25	0,0	
D26	90,0	
D27	136,0	
D28	50,6	
D29	180,0	
D30	0,0	
D31	46,0	
B26	3,5	
B23	3,5	Fixed V-F distance
A1	90,0	Fixed X _{centroid} -V-X angle